NASA Technical Memorandum 88281

Aircraft Parameter Estimation

AIAA Dryden Lecture in Research for 1987

Kenneth W. Iliff

January 1987

National Aeronautics and
Space Administration

NASA Technical Memorandum 88281

Aircraft Parameter Estimation

AIAA Dryden Lecture in Research for 1987

Kenneth W. Iliff
Ames Research Center, Dryden Flight Research Facility, Edwards, California

1987

National Aeronautics and
Space Administration
Ames Research Center
Dryden Flight Research Facility
Edwards, California 93523-5000

AIRCRAFT PARAMETER ESTIMATION*

AIAA DRYDEN LECTURE IN RESEARCH FOR 1987

Kenneth W. Iliff**
NASA Ames Research Center
Dryden Flight Research Facility
Edwards, California

Abstract

The aircraft parameter estimation problem is used to illustrate the utility of parameter estimation, which applies to many engineering and scientific fields. Maximum likelihood estimation has been used to extract stability and control derivatives from flight data for many years. This paper presents some of the basic concepts of aircraft parameter estimation and briefly surveys the literature in the field. The maximum likelihood estimator is discussed, and the basic concepts of minimization and estimation are examined for a simple simulated aircraft example. The cost functions that are to be minimized during estimation are defined and discussed. Graphic representations of the cost functions are given to illustrate the minimization process. Finally, the basic concepts are generalized, and estimation from flight data is discussed. Some of the major conclusions for the simulated example are also developed for the analysis of flight data from the F-14, highly maneuverable aircraft technology (HiMAT), and space shuttle vehicles.

Nomenclature

A, B, C, D, F, G	system matrices
a_y	lateral acceleration, g
C_ℓ	coefficient of rolling moment
C_m	coefficient of pitching moment
C_n	coefficient of yawing moment
$C_{n_{\beta_{dyn}}}$	equivalent dynamic directional stability
C_Y	coefficient of sideforce
$f(\cdot)$, $g(\cdot)$	general functions
GG*	measurement noise covariance matrix
H	approximation to the information matrix
I_x, I_y, I_z, I_{xz}	moment of inertia about subscripted axis, slug-ft^2
J	cost function
L	rolling moment divided by I_x, deg/sec^2; or, iteration number
L'	rolling moment, ft-lb
L_{YJ}	rolling moment due to yaw jet, ft-lb per jet
M	Mach number
N	number of time points or cases
n	state noise vector; or, number of unknowns
p	roll rate, deg/sec
$\bar{q}$	dynamic pressure, lb/ft^2
Re	Reynolds number
r	yaw rate, deg/sec
t	time, sec
u	control input vector
V	total velocity, ft/sec
x	state vector
z	observation vector
$\tilde{z}$	predicted Kalman-filtered estimate
α	angle of attack, deg
β	angle of sideslip, deg
Δ	time sample interval, sec
δ	control deflection, deg
δ_a	aileron deflection, deg
δ_{DE}	differential elevon deflection, deg
δ_r	rudder deflection, deg
η	measurement noise vector
μ	mean
ξ	vector of unknowns
σ	standard deviation
τ	time, sec

*Substantial portions of this paper are taken from two publications of the author, Refs. 1 and 2.

**Chief, Fluid and Flight Mechanics Branch. AIAA Fellow.

ϕ	transition matrix; or, bank angle, deg
ψ	integral of transition matrix

Subscripts

p, r, α, β, δ_a, δ_{DE}, δ_r	partial derivative with respect to subscripted variable
0	bias; or, at time zero
min	minimum value

Superscripts

~	predicted estimate
^	estimate
*	transpose

Introduction

It is difficult to present a topic as specialized as aircraft parameter estimation in a way that will interest a generalized audience of mathematicians, scientists, and engineers. The approach here is to portray parameter estimation as a specialized "curve-fitting" technique that can be applied to a broad class of problems. Much effort is expended in a variety of disciplines on a form of curve fitting, more specifically, the correlation of observed or inferred data with an assumed (though perhaps in a high- or infinite-dimensional space) mathematical model that is based on phenomenological considerations. This broad class of problems is referred to as system identification.

The application of system identification, sometimes referred to as the inverse problem (paraphrased as, Given the answer, what is the question?), presumably goes back to prehistoric times as humanity tried to master the environment by understanding, based on observation, certain phenomena (probably simple ones). Many of the physical laws stated by the Chinese, Egyptians, and Greeks were based on the same principles as are currently used in system identification. Through advancing technology and mathematical rigor, we can apply much more sophisticated techniques for making observations and for deducing the underlying phenomenology, but the basic problem of system identification remains the same.

For most physical systems, information about the general form of the system to be identified often can be derived from knowledge of the system. The most widely applied subfield of system identification is parameter identification, where the form of the mathematical model is assumed to be known. The model (an explicit function, a polynomial expansion, a look-up table, a finite-state machine defined for application of artificial intelligence, or many other forms) contains a finite number of parameters, the values of which need to be deduced or identified from the observations. One of the favored forms of the model for the most successful application is the state-space form (a rigorous treatment of state-space forms is given in Ref. 3). State-space models are very useful for dynamic systems, in which responses are time functions. Autoregressive moving average (ARMA) models are also widely known; however, discrete-time ARMA models can readily be rewritten as linear state-space models,[4] so the discussion of state-space models presented in this paper is applicable to ARMA models.

An assumed model will not be an exact representation of the system no matter how carefully its form is selected. The experimental data will not be consistent with the assumed model for any parameter values. The model may be close but will not be exact, if only because the measurements or observations will be made with real, thus imperfect, sensors. Errors in observations and in the model need to be evaluated in determining the unknown parameters of the model. So the objective becomes the application of the "best" model (in some sense), instead of the correct model, to find the "best" estimates of the unknown parameters; this process is referred to as parameter estimation. The currently favored approach to parameter estimation, and the one discussed in this paper, is to minimize the error, in the least squares sense, between the model response and the actual measured response; the estimates resulting in the minimum error are the "best" estimates. The theoretical formulation[5] and application[6] of the output error technique (which is a maximum likelihood technique that is used throughout this paper) have been thoroughly documented.

Although the applications described in this paper pertain to aircraft, the techniques have been successfully applied in other fields where the mathematical model and observations are adequate. Parameter estimation may sound like one more arcane subject, but it has application in any field where observations must be made to agree with the assumed physics of a problem. There are many obvious applications in a variety of fields, such as, spacecraft dynamics, gravitational perturbations, fluid dynamics and mechanics, optimal control, and guidance.

The application of the maximum likelihood technique for parameter estimation of aircraft coefficients demonstrates a successful application of system identification technology. Analysts in the aircraft community accept and use system identification techniques on a routine basis. Although there are isolated problems (primarily in extending the application to more difficult flight regimes, such as where the aircraft is dominated by poorly understood separated flow), there is little doubt that the basic application is highly successful. Contributing to this success are a well-understood, time-tested,[7,8] physically derived model form that is reasonably representative of the true vehicle in most flight regimes; high-quality measurements of several relevant states; the ability to apply inputs specifically for system identification; and engineers familiar with system identification, aerodynamics, aircraft equations of motion, and the associated aerodynamic coefficients.

This paper first presents a brief survey of the contributions to system identification, and specifically aircraft parameter estimation, up to 1980, when the maximum likelihood technique began to completely dominate the field. (Refs. 6 and 9

give a broad view of contributions since 1980. Ref. 9 is a bibliography of nearly 500 books, papers, and reports related to parameter estimation.) Some common uses of the estimated parameters are then discussed. The technique used for parameter estimation is then described, followed by an examination of the computational details and cost functions involved in error minimization. Finally, applications of the technique for improving high-performance aircraft and the space shuttle are described.

History of Parameter Estimation to 1980

General System Identification

The transition from hit-and-miss, rule-of-thumb system identification to mathematically sound approaches has been gradual; certainly no single germinal work can be referenced. Gauss,[10] in 1809, discussed the inverse (system identification) problem and suggested some statistical approaches that are relevant even today. The discussions of Douglas,[11] in 1940, and Gelfand and Levitan,[12] in 1951, pertaining to the inverse problem certainly qualify as truly significant works contributing to the state of the art. The formulation by Feldbaum,[13] one of the more significant works aimed at the current direction of investigation, is somewhat different than others discussed, but he did look at identification and control of the system as a single problem, the "dual control" problem. During the 1960s, a plethora of publications was evidence of increased interest in problems of this type. Much of this interest was stimulated by the well-known early works of Kalman.

The bulk of general system identification theory and application up to 1980 has been summarized in several excellent survey papers.[14-17]

The system identification problem can be divided into two major subsets: deterministic (without state noise) and nondeterministic (with state noise). There are two classes of techniques for identification of nondeterministic systems: the Kalman filter (or more generally, the extended Kalman filter) technique and the maximum likelihood technique. Many precise applications do not truly fall into these classes, but they do tend to mimic one of the two techniques. The extended Kalman filter (discussed by Åström[18] and Kashyap[19]) has been widely applied; however, this paper primarily examines the maximum likelihood estimator, proposed by Balakrishnan[20-22] and developed in Refs. 23 and 24.

Aircraft Identification

In the following chronological survey of investigations that led to the development and widespread acceptance of the maximum likelihood estimation technique for aircraft coefficient estimation, the more straightforward deterministic analysis is discussed first, followed by a brief discussion of nondeterministic analysis. Some of the investigations in estimation of unknown coefficients from aircraft dynamic response data are contained in Refs. 25 and 26. The National Advisory Committee on Aeronautics (NACA) had been publishing reports on stability derivatives (coefficients of the differential equations of motion) since the early 1920s. (The reports by Norton[7,8] involved the identification of frequency and damping ratios from flight data.)

Deterministic Analysis. The sophistication and complexity of the methods used to estimate unknown coefficients from aircraft dynamic flight responses have increased over the past 40 years. In the late 1940s and early 1950s the frequency response methods (including steady-state oscillator analysis[27] and Fourier analysis[28]) increased in popularity in aircraft analysis and in other applications. These methods yield the frequency response of the vehicle but not the coefficients of the differential equations. Attempts were made to extract these coefficients by selecting values of the aircraft coefficients that resulted in the best fit of the frequency response.[29,30] Regression techniques, such as linear least squares[31] and weighted least squares[30] techniques, were also applied to flight data at about that time. Unfortunately, regression techniques give poor results in the presence of measurement noise and yield biased estimates. The time vector technique[32] has also been applied to flight data; however, it yields an incomplete set of coefficients, and the types of responses that can be analyzed are restricted to fairly simple motions. Analog matching techniques[32,33] (time consuming and somewhat tedious) have also been applied to flight data but are limited because resulting estimates vary with the skill and technique of the operator. Comparisons of these early techniques[34,35] showed that a more complete method of identification was needed.

In 1968, two independent studies[36,37] of nonlinear minimization methods (output error methods) for obtaining aerodynamic coefficients were published, one describing the maximum likelihood estimator[36,38] (with a Gauss-Newton technique) to obtain a complete set of aerodynamic coefficients from flight data and the other describing a quasilinearization technique[37,39] to estimate some coefficients of an aircraft. One reason for the early success of these two methods is that previous research had furnished a well-defined model that adequately described the resulting motion of the vehicle. These two early results of aircraft identification by nonlinear minimization renewed interest in analysis of flight data. There was a later modification to these techniques to include *a priori* information.[40] The minimization of this modified cost functional does not result in a maximum likelihood estimator, because it is based on the joint probability distribution rather than the conditional probability. Other successful computer programs have been reported.[41-44] Extensive experience at many installations[25,26,45-58] had been obtained using the maximum likelihood estimator technique on dynamic flight responses.

Another approach, similar to these output error methods, was the application of the Kalman filter[59] to estimate the aerodynamic coefficients.

Some of the early results obtained by the Kalman filter technique were unsatisfactory; that is, the estimates of both the states and the parameters were biased and did not always converge to reasonable results. Improved results were obtained by adding the derivative of the state.[60] A weakness of the Kalman filter method is its dependence on the covariance matrix obtained from the filter.[60] However, a technique was developed for obtaining estimates of the covariance matrix with a suboptimal Kalman filter.[59] A successful application of the Kalman filter to provide the state estimates used for the estimation of stability and control derivatives and performance parameters was subsequently described.[61,62]

Nondeterministic Analysis. As previously mentioned, two classes of techniques were offered for the estimation of systems with measurement and state noise: the Kalman filter (or more generally, the extended Kalman filter) technique[18,19,59,60,63,64] and the maximum likelihood technique.[21-23,65,66] The maximum likelihood estimator for the nondeterministic case is usually referred to as the filter error method.

The general application of the extended Kalman filter was discussed in Refs. 18 and 19. The extended Kalman filter for the discrete-time case was applied to simulated aircraft data with a state noise input.[60] A similar application[63] to aircraft flight response data gave inconclusive results because the state noise input was small and the system was nonlinear. Somewhat better results were obained with an application of a greatly simplified extended Kalman filter technique.[64]

The maximum likelihood estimator was applied to response data of an aircraft flying in atmospheric turbulence;[23] the resulting coefficients were in agreement with results obtained for the same aircraft flying in smooth air, that is, without state noise.

Most of the results presented in this paper are based on an output error method program;[67] the Iliff-Maine code of this program is capable of using the Maine-Iliff formulation[68] (which can account for effects of state noise), although this feature is not used for the examples in this paper.

Basic Uses of Flight-Determined Coefficients

The extraction of unknown aerodynamic coefficients or stability and control derivatives from flight data has been of interest for many years.[7,8] The coefficients are used to provide final verification of the predicted full-scale design and to assist in the flight testing and verification of overall aircraft system performance.[1,45] After the analysis of the flight test data, the aircraft coefficients can be compared with calculated coefficients, estimates from computational fluid dynamics, and wind tunnel predictions, and these comparisons can be used to update prediction methods for the improvement of future aircraft designs.[1,46] Once an aircraft is built, the coefficients play an important role in the expansion of the flight test envelope.[1,47] As estimates of the derivatives become available, they are used to upgrade fixed-based simulators to assist in flight planning and aircraft control system modification.[1,48] In addition, the flight-determined coefficients can be used to establish compliance with the desired design specifications. Flight-determined coefficients are also used to establish the accuracy of airborne simulations[49] and to identify aircraft parameters for adaptive control.[23]

Definition of Estimation Technique

The parameter estimation problem can be defined quite simply in general terms. The system under investigation is assumed to be modeled by a set of dynamic equations containing unknown parameters. To determine the values of the unknown parameters, the system is excited by a suitable input, and the input and actual system response are measured. The values of the unknown parameters are then inferred based on the requirement that the model response to the given input match the actual system response. When formulated in this manner, the unknown parameters can be identified easily by many methods; however, complicating factors arise when application to a real system is considered.

The first complication is the impossibility of obtaining perfect measurements of the response of any real system. The inevitable sensor errors are usually included as additive measurement noise in the dynamic model, and the theoretical nature of the problem then changes drastically. It becomes impossible to identify exactly the values of the unknown parameters; instead, the values must be estimated by some statistical criterion. The theory of estimation in the presence of measurement noise is relatively straightforward for a system with discrete time observations, requiring only basic probability.

The second complication of real systems is the presence of state noise. State noise is random excitation of the system from unmeasured sources, the standard example for the aircraft stability and control problem being atmospheric turbulence. If state noise is present and measurement noise is neglected, the analysis results in the regression algorithm.[6]

When both state and measurement noise are considered,[68] the problem is more complex than in the cases that have only state noise or only measurement noise.

The final complication for real systems is modeling. It has been assumed throughout this discussion that for some value (called the best value) of the unknown parameter vector, the system is correctly described by the dynamic model. Physical systems are seldom described exactly by simple dynamic models, so the question of modeling error arises. No comprehensive theory of modeling error is available. The most common approach is to ignore it; any modeling error is simply treated as state noise or measurement noise, or both, in spite of the fact that the modeling error may be

deterministic rather than random. The assumed noise statistics can then be adjusted to include the contribution of the modeling error. This procedure is not rigorously justifiable, but combined with a carefully chosen model, it is probably the best approach available.

It is possible to make a more precise, mathematically probabilistic statement of the parameter estimation problem. The first step is to define the general system model (aircraft equations of motion), which can be written in the continuous-discrete form as

$$x(t_0) = x_0 \tag{1}$$

$$\dot{x}(t) = f[x(t), u(t), \xi] + F(\xi)n(t) \tag{2}$$

$$z(t_i) = g[x(t_i), u(t_i), \xi] + G(\xi)n_i \tag{3}$$

where x is the state vector, z is the observation vector, f and g are system state and observation functions, u is the known control input vector, ξ is the vector of unknown parameters, n is the state noise vector, n is the measurement noise vector, F and G are system matrices, t is time, and $\cdot$ denotes derivative with respect to time. The state noise vector is assumed to be zero-mean white Gaussian and stationary, and the measurement noise vector is assumed to be a sequence of independent Gaussian random variables with zero mean and identity covariance. For each possible estimate of the unknown parameters, a probability that the aircraft response time histories attain values near the observed values can then be defined. The maximum likelihood estimates are defined as those that maximize this probability. Maximum likelihood estimation has many desirable statistical characteristics; for example, it yields asymptotically unbiased, consistent, and efficient estimates.[38]

If there is no state noise, then the maximum likelihood estimator minimizes the cost function

$$J(\xi) = \frac{1}{2}\sum_{i=1}^{N}[z(t_i) - \tilde{z}_\xi(t_i)]^*(GG^*)^{-1} \times [z(t_i) - \tilde{z}_\xi(t_i)] + \frac{1}{2}N \ln|(GG^*)| \tag{4}$$

where GG^* is the measurement noise covariance matrix, $\tilde{z}_\xi(t_i)$ is the predicted response estimate of z at t_i for a given value of the unknown-parameter vector ξ (with $\sim$ denoting predicted estimate), N is the number of time points, and * denotes transpose. The cost function is a function of the difference between the measured and computed time histories.

If Eqs. (2) and (3) are linearized (as is the case for the stability and control derivatives in the aircraft problem),

$$x(t_0) = x_0 \tag{5}$$

$$\dot{\tilde{x}}(t) = Ax(t) + Bu(t) + Fn(t) \tag{6}$$

$$z(t_i) = Cx(t_i) + Du(t_i) + Gn_i \tag{7}$$

where A, B, C, and D are system matrices. For the no-state-noise case, the $\tilde{z}_\xi(t_i)$ term of Eq. (4) can be approximated by

$$\tilde{x}_\xi(t_0) = x_0(\xi) \tag{8}$$

$$\tilde{x}_\xi(t_{i+1}) = \phi\tilde{x}_\xi(t_i) + \psi[u(t_i) + u(t_{i+1})]/2 \tag{9}$$

$$\tilde{z}_\xi(t_i) = C\tilde{x}_\xi(t_i) + Du(t_i) \tag{10}$$

where the transition matrix ϕ and the integral of the transition matrix, ψ, are given by

$$\phi = \exp[A(t_{i+1} - t_i)] \tag{11a}$$

$$\psi = \int_{t_i}^{t_{i+1}} \exp(A\tau)\, d\tau\, B \tag{11b}$$

When state noise is important, the estimator based on the nonlinear form of Eqs. (1) to (3) is intractable, and ad hoc techniques are required.[69]

To minimize the cost function $J(\xi)$, we can apply the Newton-Raphson algorithm (or some other minimization technique), which chooses successive estimates of the vector of unknown coefficients, $\hat{\xi}$ ($\hat{}$ denoting estimate). If L is the iteration number, then the L + 1 estimate of ξ is obtained from the L estimate as

$$\hat{\xi}_{L+1} = \hat{\xi}_L - [\nabla^2_\xi J(\hat{\xi}_L)]^{-1}[\nabla^*_\xi J(\hat{\xi}_L)] \tag{12}$$

If $(GG^*)^{-1}$ is assumed fixed, the first and second gradients are defined as

$$\nabla_\xi J(\xi) = -\sum_{i=1}^{N}[z(t_i) - \tilde{z}_\xi(t_i)]^*(GG^*)^{-1}[\nabla_\xi \tilde{z}_\xi(t_i)] \tag{13}$$

$$\nabla^2_\xi J(\xi) = \sum_{i=1}^{N}[\nabla_\xi \tilde{z}_\xi(t_i)]^*(GG^*)^{-1}[\nabla_\xi \tilde{z}_\xi(t_i)] - \sum_{i=1}^{N}[z(t_i) - \tilde{z}_\xi(t_i)]^*(GG^*)^{-1}[\nabla^2_\xi \tilde{z}_\xi(t_i)] \tag{14a}$$

The Gauss-Newton approximation to the second gradient is

$$\nabla^2_\xi J(\xi) \cong \sum_{i=1}^{N}[\nabla_\xi \tilde{z}_\xi(t_i)]^*(GG^*)^{-1}[\nabla_\xi \tilde{z}_\xi(t_i)] \tag{14b}$$

The Gauss-Newton approximation is computationally much easier than the Newton-Raphson method because the second gradient of the innovation never needs

to be calculated. In addition, it can have the advantage of speeding the convergence of the algorithm, as is discussed in Ref. 6.

Figure 1 illustrates the maximum likelihood estimation concept. The measured response is compared with the estimated response, and the difference between these responses is called the response error. The cost functions of Eqs. (4) and (11) include this response error. The minimization algorithm is used to find the coefficient values that minimize the cost function. Each iteration of this algorithm provides a new estimate of the unknown coefficients on the basis of the response error. These new estimates of the coefficients are then used to update values of the coefficients of the mathematical model, providing a new estimated response and therefore a new response error. The updating of the mathematical model continues iteratively until a convergence criterion is satisfied. The estimates resulting from this procedure are the maximum likelihood estimates.

The maximum likelihood estimator also provides a measure of the reliability of each estimate based on the information obtained from each dynamic maneuver. This measure of the reliability, analogous to the standard deviation, is called the Cramér-Rao bound[5,24] or the uncertainty level. The Cramér-Rao bound as computed by current programs should generally be used as a measure of relative accuracy rather than absolute accuracy. The bound is obtained from the approximation to the information matrix, H, which is based on Eq. (14b); the actual information matrix is defined when evaluated at the correct values (not maximum likelihood estimates) of all the coefficients. The bound for each unknown is the square root of the corresponding diagonal element of H^{-1}; that is, for the ith unknown, the Cramér-Rao bound is $\sqrt{H^{-1}(i,i)}$.

The formulation and the minimization algorithm previously discussed (Eqs. (4) to (14)) are implemented with the Iliff-Maine code (MMLE3 maximum likelihood estimation program). The program and computational algorithms are described fully in Ref. 67. All the computations shown and described in the remainder of this paper use the algorithms exactly as described in Ref. 67.

Simple Simulated Example

For the discussion that follows, some knowledge of differential equations is assumed. A full derivation and a discussion of the aircraft equations of motion are given in Ref. 6.

The basic concepts involved in a parameter estimation problem will be illustrated by a simple simulated example representative of a realistic problem: an aircraft that exhibits pure rolling motion from an aileron input. This example, although simplified, typifies the motion exhibited by many aircraft in particular flight regimes, such as the F-14 aircraft flying at high dynamic pressure, the F-111 aircraft at moderate speed with the wing in the forward position, and the T-37 aircraft at low speed.

Derivation of an equation describing this motion is straightforward. Figure 2 illustrates an aircraft with the x axis perpendicular to the plane of the figure (positive forward on the aircraft). The rolling moment L', roll rate p, and aileron deflection δ are positive as shown. For this example, the only state is p, and the only control is δ. The result of summing moments is

$$I_x\dot{p} = L'(p, \delta) \tag{15}$$

where I_x is the rolling moment about the subscripted (x) axis. The first-order Taylor expansion then becomes

$$\dot{p} = \frac{\partial L}{\partial p} dp + \frac{\partial L}{\partial \delta} d\delta \tag{16}$$

assuming small perturbations and using the notation

$$\dot{p} = L_p p + L_\delta \delta \tag{17}$$

where

$$L = L'/I_x$$

and the subscripts p and δ denote partial derivative with respect to the subscripted variable.

Equation (17) is a simple aircraft equation where the forcing function is provided by the aileron and the damping by the damping-in-roll term L_p. In subsequent sections we examine in detail the parameter estimation problem where Eq. (17) describes the system. For this single-degree-of-freedom problem, the maximum likelihood estimator is used to estimate L_p or L_δ, or both, for a given simulated time history.

We will assume that the system has measurement noise but no state noise; therefore, we can use Eqs. (1) to (3). Equation (4) then gives the cost function for maximum likelihood estimation. The weighting $(GG^*)^{-1}$ is unimportant for this problem, so let $GG^* = 1$. For our example,

$$\begin{aligned} x_i &= p_i \\ z_i &= x_i \end{aligned} \tag{18}$$

Therefore, Eq. (4) becomes

$$J(L_p, L_\delta) = \frac{1}{2} \sum_{i=1}^{N} [p_i - \tilde{p}_i(L_p, L_\delta)]^2 \tag{19}$$

where p_i is the value of the simulated measured response p at time t_i and $\tilde{p}_i(L_p, L_\delta)$ is the estimated time history of $\tilde{p}$ at time t_i for $L_p = \hat{L}_p$

and $L_\delta = \hat{L}_\delta$. Throughout the rest of this paper, where simulated data (not experimental flight data) are used, the simulated measured time history refers to p_i, and the estimated computed time history, which varies with each iteration, is $\tilde{p}_i(L_p, L_\delta)$. The estimated time history is a function of the current estimates of L_p and L_δ, but the simulated measured time history, p_i, is not.

The most straightforward method of obtaining $\tilde{p}_i$ is with Eqs. (8) and (9). Using the previously stated notation,

$$\tilde{p}_{i+1} = \phi\tilde{p}_i + \psi(\delta_i + \delta_{i+1})/2 \tag{20}$$

where

$$\phi = \exp(L_p\Delta) \tag{21}$$

$$\psi = \int_0^\Delta \exp(L_p\tau)\, d\tau\, L_\delta = \frac{L_\delta[1 - \exp(L_p\Delta)]}{L_p} \tag{22}$$

and Δ is the length of the sample interval, $t_{i+1} - t_i$.

The maximum likelihood estimate is obtained by minimizing the cost function (Eq. (19)), which is done by applying the Gauss-Newton method. Equation (12) is used to determine successive vof the estimates of the unknowns during the minimization.

For this simple problem, $\hat{\xi} = [\hat{L}_p \quad \hat{L}_\delta]^*$, and successive values of $\hat{L}_p$ and $\hat{L}_\delta$ are determined by updating Eq. (12). The first and second gradients of Eq. (12) are defined by Eqs. (13) and (14b).

We now can write the entire procedure for obtaining the maximum likelihood estimates for this simple example. To start the algorithm, initial estimates of L_p and L_δ are needed to define the value $\hat{\xi}_0$. Using Eq. (12), $\hat{\xi}_1$ and subsequently $\hat{\xi}_L$ are defined by using the first and second gradients of $J(L_p, L_\delta)$ from Eq. (19). The gradients for this particular example, from Eqs. (13) and (14b), are

$$\nabla_\xi J(\hat{\xi}_L) = -\sum_{i=1}^{N} (p_i - \tilde{p}_i)\nabla_\xi\tilde{p}_i \tag{23}$$

$$\nabla_\xi^2 J(\hat{\xi}_L) \cong \sum_{i=1}^{N} (\nabla_\xi\tilde{p}_i)^*\nabla_\xi\tilde{p}_i \tag{24}$$

Computational Details of Minimization

In the previous section we specified the equations for a simple example and described the procedure for obtaining estimates of the unknowns from a dynamic maneuver. In this section we give the computational details for obtaining the estimates. Some of the basic concepts of parameter estimation are best shown with simulated measured data, where the best (correct, in this simulated case) answers are known. Therefore, in this section we study two examples involving simulated time histories. The first example is based on data that have no measurement noise, which results in estimates that are the same as the correct values. The second example contains significant measurement noise; consequently, the estimates are not the same as the correct values.

For this simulated example, 10 points (time samples) are used. The simulated measured data, which we refer to as the measured data, are based on Eq. (17). We use the same correct values $L_p = -0.2500$ and $L_\delta = 10.0$ for both examples. In addition, the same input δ is used for both examples, the sample interval $\Delta = 0.2$ sec, and the initial conditions are zero. Tables of all the significant intermediate values of the calculations are given in Ref. 6. In both examples, the initial values defining $\hat{\xi}_0$ are $L_p = -0.5$ and $L_\delta = 15.0$.

Example With No Measurement Noise. The simulated measured time history of aileron deflection for the case with no measurement noise (no-noise case) is shown in Fig. 3. The aileron input starts at zero, goes to a fixed value, and then returns to zero. The resulting simulated measured roll rate time history is also shown.

Table 1 gives the values for $\hat{L}_p$, $\hat{L}_\delta$, and J for each iteration, along with the values of ϕ and ψ needed for calculating $\tilde{p}_i$. In three iterations the algorithm converges to the correct values to four significant digits for both L_p and L_δ.

Figure 4 shows the match between the simulated measured data and the estimated data for each of the first three iterations. The match is very close after two iterations and is nearly exact after three.

Although the algorithm converges to four-digit accuracy in L_p and L_δ, the value of the cost function J continues to decrease rapidly between iterations 3 and 4. This is a consequence of using the maximum likelihood estimator on data having no measurement noise. Theoretically, with infinite accuracy the value of J at the minimum should be zero. However, with finite accuracy the value of J becomes small but never reaches zero. This value is a function of the number of significant digits. For the 13-digit accuracy used here, the cost eventually decreases to approximately 0.3×10^{-28}.

Example With Measurement Noise. The simulated measured data used in the case with measurement noise (noisy case) are the same as those used in the previous section, except that pseudorandom Gaussian noise is added to the roll rate (Fig. 5). The signal-to-noise ratio is quite low in this example (compare Figs. 3 and 5). The values of $\hat{L}_p$, $\hat{L}_\delta$, ϕ, ψ, and J for each iteration are given in Table 2. The algorithm converges in four iterations. The behavior of the coefficients as

they approach convergence is much like that in the no-noise case. The most notable result of this case is that the converged values of L_p and L_δ are somewhat different from the correct values. The match between the simulated measured and estimated time histories is shown in Fig. 6 for each iteration. No change in the match is apparent for iterations 2 and 3. The match is very good considering the amount of measurement noise.

In Fig. 7, the time history estimated using the no-noise estimates of L_p and L_δ is compared with that using the noisy estimates of L_p and L_δ. Because the algorithm converged to values somewhat different from the correct values, the two estimated time histories for their respective values are similar but not identical.

The accuracy of the converged elements can be assessed by looking at the Cramér-Rao inequality[24,67] discussed previously. The Cramér-Rao bound can be obtained from an approximation to the information matrix H, where

$$H^{-1} = 2J_{min}\left\{\sum_{i=1}^{N}[\nabla_\xi \tilde{z}_\xi(t_i)]^*(GG^*)^{-1}\nabla_\xi \tilde{z}_\xi(t_i)\right\}^{-1}/(N-1)$$

The Cramér-Rao bounds for L_p and L_δ are the square roots of the diagonal elements of the H^{-1} matrix, or $\sqrt{H^{-1}(1,1)}$ and $\sqrt{H^{-1}(2,2)}$, respectively. The Cramér-Rao bounds are 0.1593 and 1.116 for L_p and L_δ, respectively. The differences between $\hat{L}_p$ and L_p and between $\hat{L}_\delta$ and L_δ are less than their respective bounds.

Cost Functions

In the previous section we obtained the maximum likelihood estimates for simulated time histories by minimizing the values of the cost functions. To fully understand what occurs in this minimization, we must study in more detail the form of the cost functions and some of their more important characteristics. In this section, the cost function for the no-noise case is discussed briefly. The cost function for the noisy case is then discussed in more detail. The same two time histories studied in the previous section are examined here. The noisy case is more interesting because it has a meaningful Cramér-Rao bound and is more representative of aircraft flight data.

It is important to remember that in this paper everything related to cost functions (Eq. (19)) is based on simulated time histories that are defined by Eq. (17). For every measured time history we might choose (simulated or flight data), a complete cost function is defined. For the case of n variables, the cost function defines a hypersurface of n + 1 dimensions. We could avoid bothering with the minimization algorithm if we could construct this surface and look for the minimum, but this is not a reasonable approach, because the number of variables is generally greater than two. Therefore, the cost function can be described mathematically but not pictured graphically.

One-Dimensional Case. To illustrate the many aspects of cost functions, it is easiest to look first at cost functions having one variable. In an earlier section, the cost function of L_p and L_δ was minimized. That cost function is most interesting in the L_p direction. Therefore, the one-variable cost function studied here is $J(L_p)$, with the correct value of L_δ = 10.0. Figure 8 shows the cost function plotted as a function of L_p for the no-noise case. As expected for this case, the minimum cost is zero and occurs at the correct value of L_p = -0.2500. It is apparent that the cost increases much more slowly for a more negative L_p than for a positive L_p. In fact, the slope of the curve tends to become less negative where $L_p < -1.0$. Physically this makes sense because the more negative values of L_p represent cases of high damping and the positive L_p represents an unstable system. Therefore, the p_i for positive L_p becomes increasingly different from the measured time history for small positive increments in L_p. For very large damping (very negative L_p), the system would show essentially no response. Therefore, further large increases in damping result in relatively small changes in the value of $J(L_p)$.

In Fig. 9, the cost function based on the noisy case time history is plotted as a function of L_p. The correct L_p value (-0.2500) and the L_p value (-0.3218) at the minimum of the cost (3.335) are both indicated on the figure. The general shape of the cost function in Fig. 9 is similar to that shown in Fig. 8. Figure 10 compares the cost functions based on the noisy and no-noise cases. The comments relating to the cost function based on the no-noise case also apply to the cost function based on the noisy case. Figure 10 shows clearly that the two cost functions are shaped similarly but shifted in both the L_p and J directions. Only a small difference in the value of the cost would be expected far from the minimum because the "estimated" time history is so far from the simulated measured time history that it becomes irrelevent as to whether the simulated measured time history has noise added. Therefore, for large values of cost, the difference in the two cost functions should be small compared with the total cost.

Figure 11 shows the gradient of $J(L_p)$ plotted as a function of L_p for the noisy case. Finding the zero of this function (or equivalently, the minimum of the cost function) using the Gauss-Newton method was discussed previously. The gradient is zero at L_p = -0.3218, which corresponds to the value of the minimum of $J(L_p)$.

The usefulness of the Cramér-Rao bound was discussed in the Example With Measurement Noise section. It is useful to digress briefly to discuss some of the ramifications of the Cramér-Rao bound for the one-dimensional case. The Cramér-Rao bound has meaning only for the noisy case. In the noisy example, the estimate of L_p is -0.3218, and the Cramér-Rao bound is 0.0579. The calculation of the Cramér-Rao bound was

defined in the previous section for both the one-dimensional and the two-dimensional examples. The Cramér-Rao bound is an estimate of the standard deviation of the estimate. The scatter in the estimates of L_p should be of about the same magnitude as the estimate of the standard deviation. For the one-dimensional case discussed here, the range (L_p = -0.3218 plus or minus the Cramér-Rao bound, 0.0579) nearly includes the correct value L_p = -0.2500. If noisy cases are generated for many time histories (adding different measurement noise to each time history), then the sample mean and sample standard deviation of the estimates for these cases can be calculated. Table 3 gives the sample mean μ, sample standard deviation σ, and the standard deviation of the sample mean, $\sigma/\sqrt{N}$, for 5, 10, and 20 cases. The sample mean, as expected, gets closer to the correct value of -0.2500 as the number of cases increases. This is also reflected in the table by the decreasing values of $\sigma/\sqrt{N}$, which are estimates of the error in the sample mean. The sample standard deviations indicate the approximate accuracy of the individual estimates. This standard deviation, which stays more or less constant, is approximately equal to the Cramér-Rao bound for the noisy case being studied here. In fact, the Cramér-Rao bounds of the 20 noisy cases used here (not shown in the table) do not change much from the values found for the particular noisy case being studied. Both of these results are in good agreement with the theoretical characteristics[24] of the Cramér-Rao bounds and maximum likelihood estimators in general.

These examples indicate the value of obtaining more sample time histories (experiments or, in an aircraft example, dynamic maneuvers). Having more samples improves confidence in the estimate of the unknowns. This also holds true in analyzing actual flight time histories (maneuvers); thus, it is always advisable to obtain data from several maneuvers at a given flight condition to improve the best estimate of each derivative.

The magnitudes of the Cramér-Rao bounds and of the error between the correct and estimated values of L_p are determined largely by the length of the time history and the amount of noise added to the correct time history. For the case being studied, it is apparent from Fig. 5 that a large amount of noise is added to the time history. The effect of the measurement noise power (GG*, Eqs. (3) and (4)) on the estimate of L_p for the time history is indicated in Table 4. The estimate of L_p is much improved by decreasing the measurement noise power. A reduction in the value of G to one-tenth of the value in the noisy case being studied yields an acceptable estimate of L_p. For real data, the measurement noise is reduced by improving the accuracy of the sensor outputs.

Two-Dimensional Case. In this section, the cost function dependent on both L_p and L_δ is studied. The no-noise case is examined first, followed by the noisy case.

Even though the cost function is a function of only two unknowns, it is much more difficult to visualize than is the one-dimensional case. The cost function over reasonable ranges of L_p and L_δ is shown in Fig. 12. The minimum must lie in the curving valley that gets broader toward the far side of the surface. The cost increases very rapidly in the region of positive L_p and large values of L_δ. The reason for this rapid increase is just an extension of the argument for positive L_p, given in the previous section. With this picture of the surface, we can look at the isoclines of constant cost on the L_p-L_δ plane (Fig. 13). The minimum of the cost function is inside the closed isocline. The steepness of the cost function in the positive L_p direction is once again apparent. The more nearly elliptical shape inside the closed isocline indicates that the cost is nearly quadratic there, so fairly rapid convergence in this region would be expected. The L_p axis becomes an asymptote for cost as L_δ approaches zero. The cost is constant for L_δ = 0 because no response would result from any aileron input; the estimated response is zero for all values of L_p, resulting in constant cost.

The region of the minimum value of the cost function (Fig. 13), as seen in the earlier example (Table 1), occurs at the correct values L_p = -0.2500 and L_δ = 10.0. This is also evident by looking at the cost function surface shown in Fig. 14. The surface has its minimum at the correct value. As expected, the value of the cost function at the minimum is zero.

As in the one-dimensional case, the primary difference between the cost functions for the no-noise and noisy cases is a shift in the cost function. In the one-dimensional case, the cost function for the noisy case was shifted so that the minimum was at a higher cost and a more negative value of L_p. In the two-dimensional case, the cost function exhibits a similar shift in both the L_p and the L_δ directions. The shift is small enough that the difference is not visible at the scale shown in Fig. 12. Figure 15 shows the isoclines of constant cost for the noisy case, which look much like the isoclines for the no-noise case shown in Fig. 13; the difference is a shift in L_p of about 0.1, the difference at the minimum for the no-noise and noisy cases. Heuristically, one can see that this would hold true for cases with more than two unknowns; the primary difference between the two cost functions is near the minimum.

The next step is to examine the cost function near the minimum. Figure 16 shows the same view of the cost function for the noisy case as shown in Fig. 14 for the no-noise case. The shape is roughly the same as that shown in Fig. 14, but the surface is shifted such that its minimum lies over L_p = -0.3540 and L_δ = 10.24, and it is shifted upward to a cost function value of approximately 3.3.

To get a more precise idea of the cost function of the noisy case near the minimum, we must once again examine the isoclines. The isoclines in this region (Fig. 17) are much more like ellipses than those in Figs. 13 and 15. The results from Table 2 are included on Fig. 17, so we can

follow the path of the minimization example used before. The first iteration (L = 1) brought the values of L_p and L_δ very close to the values at the minimum, and the second essentially arrived at the minimum (viewed at this scale). One of the reasons the convergence is so rapid in this region is that the isoclines are nearly elliptical, demonstrating that the cost function is very nearly quadratic in this region. If we had started the Gauss-Newton algorithm at a point where the isoclines are much less elliptical (as in some of the border regions in Fig. 15), the convergence would have progressed more slowly initially, but it would have progressed at much the same rate as it entered the nearly quadratic region of the cost function.

Before concluding our examination of the two-dimensional case, we shall examine the Cramér-Rao bound. Figure 18 shows the uncertainty ellipsoid, which is based on the Cramér-Rao bound. (The relationships between the Cramér-Rao bound and the uncertainty ellipsoid are discussed in Ref. 69.) The uncertainty ellipsoid almost encloses the correct values of L_p and L_δ. The Cramér-Rao bound for L_p and L_δ can be determined from the projection of the uncertainty ellipsoid onto the L_p and L_δ axes and then compared with the values calculated for the noisy case, which were 0.1593 and 1.116 for L_p and L_δ, respectively. This projection is analogous to the case for n unknowns, but in that case the projection would be the n + 1 hyperellipsoid's projection onto a hypersurface.

Estimation Using Flight Data

We have examined the basic mechanics of obtaining maximum likelihood estimates from simulated examples with one or two unknown parameters. To make the transition from theory to practical application, we present results obtained from analysis of actual flight data and discuss how the aircraft parameter estimation results are used to solve real problems. In this case we illustrate the necessity of obtaining estimates of the aircraft coefficients of the differential equations of motion (the stability and control derivatives) to solve important and related problems encountered in flight. However, the aircraft stability and control example is only one of several applications of parameter estimation techniques; useful results can be obtained in many applications where the phenomenology is well understood. For the computationally difficult situation usually encountered with actual flight data, we obtain the maximum likelihood estimates with the Iliff-Maine code (MMLE3 program).[67] Before studying the specific examples, a brief historical review of some other uses of the estimates is presented.

In the past, the primary reason for estimating stability and control derivatives from flight tests was to make comparisons with wind tunnel estimates. As aircraft became more complex and as flight envelopes were expanded to include flight regimes that were not well understood, new requirements of the derivative estimates evolved. For many years, the flight-determined derivatives were used in simulations to aid in flight planning and in pilot training. The simulations were particularly important in research flight test programs in which an expansion of the envelope into new flight regimes was required. As more was learned about these new flight regimes, the complexity of the aircraft, and particularly their sophisticated flight control systems, increased. The design and refinement of the control system for these complex aircraft required higher fidelity simulations. As a consequence, a more complete knowledge of the flight-determined stability and control derivatives was necessary. Almost all current high-performance aircraft have very complex control systems to compensate for their deficiencies in basic aerodynamic characteristics. Consequently, most flight test programs for these aircraft require a complete flight-determined set of stability and control derivatives, and parameter estimation techniques for estimating stability and control derivatives from flight data have become more sophisticated.

At the Dryden Flight Research Facility of NASA's Ames Research Center (Ames-Dryden), analysts have been involved in the estimation of stability and control derivatives with maximum likelihood estimators since 1966 and have successfully applied maximum likelihood estimators to nearly 50 different aircraft configurations. Some of the experience gained through these applications is included in the bibliography of Ref. 9. Recent Ames-Dryden applications have concentrated on estimating stability and control derivatives to assist in designing or refining control systems. Three such applications (to be discussed in detail) are the F-14, highly maneuverable aircraft technology (HiMAT), and space shuttle programs. All three of these programs have made extensive use of high-fidelity, pilot-in-the-loop simulations, which are implemented using the best wind tunnel data available. Portions of these flight test programs were defined to obtain data for refining simulator models.

The chosen method of enhancing the simulator model depends on the aircraft involved in the flight test program. The F-14 aircraft flew several flights specifically for defining the stability and control derivatives over a large angle-of-attack range because the necessary control refinement related to the high-angle-of-attack regime. The HiMAT vehicle flew several flights with a positive static margin (stable open-loop system) so that derivatives could be obtained to design a control system for flight at a negative static margin (unstable open-loop system). The space shuttle entered from space on the most conservative trajectory to allow assessment of its characteristics before an envelope expansion was begun.

Once the flight data are obtained and analyzed, the simulator is updated to assist in control system design and further flight planning. Where flight results agree with wind tunnel predictions, confidence in the simulation grows, and envelope expansion proceeds more efficiently.

The coefficients evaluated in this section are contained in the aircraft equations of motion, which are derived and discussed in detail in Ref. 6.

F-14 Aircraft

The F-14 aircraft is a twin-engine, high-performance fighter with variable wing sweep (Fig. 19). The Ames-Dryden F-14 program was intended to improve the handling qualities of the airplane at high angles of attack by incorporating several control system techniques.[70,71] The first part of the program was dedicated to obtaining flight-determined stability and control derivatives for the subsonic envelope of the F-14 aircraft, the complete trimmed angle-of-attack range for Mach number $M < 0.9$.

In many instances the flight data agreed with the wind tunnel predictions; Fig. 20 (from Ref. 70) shows the comparison of C_{n_β} (C_n being the coefficient of yawing moment) as a function of angle of attack α from flight and wind tunnel estimates. (Throughout this and following discussions, a subscript to the coefficient denotes partial derivative with respect to the subscripted variable.) The symbols denote the estimate, and the vertical bar designates the uncertainty level (Cramér-Rao bound). The agreement is good, although there is some disagreement at $\alpha > 25°$; nevertheless, the same trends are seen for both flight and wind tunnel data.

Figure 21 shows the flight-determined C_{ℓ_p} (C_ℓ being the coefficient of rolling moment) as a function of α for $M < 0.55$ and for $M = 0.9$. There was some uncertainty in the accuracy of the wind tunnel predictions of C_{ℓ_p} because the wind tunnel model configuration was different from the flight configuration. The implementation of C_{ℓ_p} at $M = 0.9$ in the simulation produced a previously unsimulated wing rock characteristic that had been observed in flight. The wing rock had been a troublesome characteristic, and its simulation was important in improving handling qualities through control system modifications. Figure 22 shows the flight-determined values of C_{ℓ_β} as a function of α compared with the results of two different sets of wind tunnel results. There had been some concern about the disagreement between the two sets of wind tunnel results before flight. At low angles of attack, the three sets of estimates are in fair agreement; however, at $\alpha > 15°$, the flight data lie between the two sets of wind tunnel data.

A last example from the F-14 aircraft shows how the wind tunnel and flight estimates interplay to improve a simulation. After the lateral-directional derivatives were incorporated in the simulation, the resulting simulated lateral-directional motions from a longitudinal-stick snap maneuver were found to be inconsistent with the flight response. Since the F-14 program was primarily a lateral-directional investigation, the longitudinal derivatives in the simulation had not been updated with the flight-determined values. When the flight-determined longitudinal derivatives were included in the simulation, the stick snap response agreed more closely with the flight response. In tracking down the inconsistency, a large discrepancy was discovered between the wind tunnel and flight-determined values of C_{m_α} (C_m being the coefficient of pitching moment). This is shown in Fig. 23, where flight-determined C_{m_α} is compared with the wind tunnel estimates of C_{m_α} for the untrimmed and trimmed conditions. Further investigation showed that the untrimmed values of C_{m_α} had been put in the simulation and that the predicted trimmed values of C_{m_α} were in excellent agreement with flight estimates.

Examples using C_{ℓ_p}, C_{ℓ_β}, and C_{m_α} show how flight data, in addition to providing a primary source of estimates, can be used to help interpret wind tunnel data; these data can then be used to improve the simulation at points away from steady-state flight data. Sometimes wind tunnel data are available but have been discounted or overlooked, and flight data can give new credence to these wind tunnel data.

These F-14 flight data improved the simulation over a large part of the envelope. Since the F-14 high-angle-of-attack program also needed to examine responses of a highly transient nature, more tedious and time-consuming fine tuning of the simulation was required for flight at other than near the trimmed conditions.[72] With the resulting simulation, the proposed control system techniques were further refined; the result was a more efficient demonstration in flight.

This exemplifies the value of flight test parameter estimation in improving the handling qualities of an aircraft through control system improvements.

HiMAT Vehicle

The HiMAT vehicle is a remotely piloted research vehicle with advanced close-coupled canards, wing-type winglets, and provisions for variable leading-edge camber. It is made of advanced composite materials to allow for aeroelastic tailoring and to minimize weight. It was flown in an unstable configuration because the wing deformation then resulted in a desirable camber shape at high load factor and because the trim drag was reduced.

The HiMAT vehicle[73,74] (Fig. 24) was designed to fly with a sustained 8-g turn capability at Mach 0.9 at 25,000 ft altitude and to demonstrate flight supersonically to Mach 1.4. To attain the Mach 0.9 condition, it was predicted that the vehicle must be flown in an unstable configuration (10-percent mean aerodynamic cord (MAC) negative static margin). The philosophy for testing the HiMAT vehicle was somewhat different from that for production aircraft: Flight-determined stability and control derivatives were to be relied on to keep the wind tunnel program to a minimum. The original simulation data base contained the wind tunnel data supplemented with some computed characteristics.

The vehicle was flown in a stable configuration to obtain stability and control derivatives with the control feedbacks set to zero. While these data were being gathered, a control

system suitable for unstable flight was being designed, based on wind tunnel tests. Then, with the flight-determined derivatives, the simulator was updated and the control system adjusted for this update so that the unstable vehicle could be flown safely. Stability and control maneuvers were performed at subsonic and supersonic Mach numbers, at angles of attack up to 10°, and at altitudes from 15,000 to 45,000 ft. A complete set of stability and control characteristics was obtained for both the longitudinal and lateral-directional degrees of freedom.[75] Because the values of the HiMAT derivatives are classified, the data are plotted on unlabeled vertical axes; nevertheless, an assessment of predicted and flight-determined derivatives can still be made. All the derivatives, predicted and flight determined, are corrected to 0-percent MAC. For the flight conditions flown, there were no aeroelastic effects noted in the flight data.

Figure 25 shows flight-determined directional dynamic stability $C_{n_{\beta_{dyn}}}$ as a function of Mach number at $\alpha = 4°$ compared with the rigid and flexible predictions. Flight estimates are about the same as predictions at M = 0.4 and 0.9, but they differ significantly in between. In Fig. 26, $C_{n_{\beta_{dyn}}}$ is plotted as a function of α at M = 0.9, showing that the vehicle is slightly unstable in the lateral-directional axes at the lower angles of attack. Considering that these data are plotted for 0-percent MAC, this instability would be considerably greater and over a wider angle-of-attack range if the center of gravity were moved significantly aft (aft movement of the center of gravity makes any vehicle less stable). The derivatives C_{Y_β} (C_Y being the coefficient of side-force) and C_{ℓ_p} agreed with predictions; however, C_{n_r} was twice the predicted value, C_{n_p} was of opposite sign, and C_{ℓ_r} was a small fraction of predictions. The rolling moments due to aileron, $C_{\ell_{\delta_{DE}}}$, agreed fairly well with the rigid predictions; $C_{n_{\delta_r}}$ was 25-percent less than predicted; both $C_{n_{\delta_a}}$ and $C_{n_{\delta_{DE}}}$ showed a positive increment over prediction. The derivative $C_{\ell_{\delta_r}}$ was about twice the predicted value. Since there were so many large differences between the flight-determined derivatives and the minimal wind tunnel set, it was decided to completely reevaluate the lateral-directional control laws designed for the unstable configuration using the flight data instead of the wind tunnel data, which were used in the original design. Some reasons for this can be seen in Fig. 27, in which the control derivatives $C_{n_{\delta_{DE}}}$, $C_{\ell_{\delta_r}}$, and $C_{n_{\delta_r}}$ are plotted as functions of α at M = 0.9. These differences between flight and predicted values meant that the simulator had to be extensively revised.

The HiMAT vehicle program was a technology demonstration program and therefore was required to demonstrate the technology only at specific design points. A technology demonstration is quite different from many programs, such as the F-14 program, because only certain steady-state requirements must be demonstrated. Therefore, all the points (or flight conditions) that needed to be flown were near steady-state points for which flight-demonstrated derivatives already existed. To update the simulator, all the predicted data were disregarded, and only flight-determined stability and control derivatives were used. The knowledge that the aircraft stability and control derivatives exhibited no significant aeroelastic effects permitted the reevaluation of the unstable control system, and the design was simplified.

The control laws designed for the unstable configuration were much more complex than the rate-feedback system used for gathering stability and control derivatives. The new control laws were modified by (1) adding a lateral acceleration a_y feedback to improve closed-loop directional dynamic stability; (2) adding an interconnect between lateral stick and rudder to improve lateral control characteristics; (3) changing the various feedback gains to improve damping characteristics; and (4) locking the aileron surface to eliminate adverse yaw and also to eliminate the possibility of a predicted surface-buzz problem at higher Mach numbers. This design of the lateral-directional control system was the result of an extensive study of possible control systems using both the simulator and the linear analysis techniques. When the new control system was designed, it was implemented on the HiMAT vehicle, and it was flown in a stable configuration. Control surface doublets were input, and the responses were compared with the simulator-derived responses. The comparison was excellent, giving confidence that the unstable vehicle could be tested.

The benefits of flying the unstable vehicle were demonstrated in flight when a 0.4-g improvement in sustained-g capability was realized by changing the center-of-gravity location from the point of neutral stability to 5-percent MAC aft of the neutral point. When the unstable vehicle was flown with a 5-percent MAC negative static margin, a sustained turn of about 7.8 g was achieved. Based on these numbers, the HiMAT vehicle should be able to demonstrate a sustained 8.0-g turn capability with the 10-percent MAC negative static margin (unstable vehicle).

In the case of the HiMAT vehicle, flight test parameter estimation became the sole method of defining the stability and control derivatives. A control system design for the unstable configuration was defined from flight test results. The adequacy of the design was demonstrated on the simulation updated with flight data. The resulting control system enabled the unstable vehicle to be flown.

A recent investigation of determining the aerodynamic coefficients for the highly unstable X-29A vehicle is described in Ref. 69. This investigation sheds new light on parameter estimation of unstable systems, which has widespread application to systems other than those defined by stability and control derivatives.

Space Shuttle Orbiter

The space shuttle orbiter is a large double-delta-winged vehicle designed to enter the atmos-

phere and land horizontally. The entry control system consists of 12 vertical reaction control system (RCS) jets (6 up-firing and 6 down-firing) and 8 horizontal RCS jets (4 left-firing and 4 right-firing), 4 elevon surfaces, a body flap, and a split rudder surface (Fig. 28). The vertical jets and the elevons are used for both pitch and roll control. The jets and elevons are used symmetrically for pitch control and asymmetrically for roll control. More information on the configuration and flight plan is given in Ref. 76.

The F-14 and HiMAT examples showed how parameter estimation can be used in an incremental flight test program, that is, a progressive expansion of the flight envelope to obtain data in the more certain areas first and in the more challenging or hazardous ones later. However, the space shuttle program could not be approached in this manner, for the vehicle had to demonstrate on the first flight that it could be flown safely over most of its envelope. Further complicating the program, this first flight included very hazardous flight regimes. The subsonic flight and landing characteristics had been demonstrated in the earlier approach and landing test program, but the hypersonic, peak heating, and transonic regions were largely unexplored for a vehicle of this type.

Extensive wind tunnel tests were performed, and those data were incorporated into high-fidelity simulations. No matter how carefully wind tunnel tests are performed, there are frequently discrepancies between the predictions and the demonstrated flight characteristics; therefore, uncertainties were defined for each stability and control derivative. These uncertainties (called variations in Ref. 77) were based to a large extent on previously reported discrepancies between predictions and flight.[78]

In preparation for the first flight, a control system was developed to provide satisfactory closed-loop vehicle characteristics for derivatives that fell between the variations that had been previously defined. After flight data were obtained, the flight estimates of the stability and control derivatives were used to reduce the preflight variations. This reduction then allowed the control engineers to refine the control system and therefore to improve the shuttle handling qualities. In addition, the flight-determined derivatives were used to determine if configuration placards (limitations on the flight envelope) could be modified or removed.

Some of the stability and control results obtained from the first three flights are contained in Refs. 79 and 80. One interesting example of where parameter estimation played an important role in the shuttle program occurred during the first energy-management bank maneuver on the first entry of the shuttle (STS-1). The response to the automated control inputs computed using the predicted stability and control derivatives is shown in Fig. 29. It should be noted that the control inputs shown here (and for all other simulation comparisons) are the closed-loop commands from the shuttle control laws. The maneuver was to be made at a velocity $V = 24{,}300$ ft/sec and at a dynamic pressure $\bar{q} \approx 12$ lb/ft^2.

The actual STS-1 maneuver that occurred at this flight condition is shown in Fig. 30, which depicts a more hazardous maneuver than was predicted. At this flight condition the excursions must be kept small. The flight maneuver resulted in twice the angle-of-sideslip β peaks predicted and in a somewhat higher roll rate than predicted. Also, there was more yaw-jet firing than was predicted, and the motion was more poorly damped than predicted. It is obvious from comparing the predicted with the actual maneuver (Fig. 31) that the stability and control derivatives were significantly different than predicted. It is fortunate that the control system design philosophy discussed previously had been used for the shuttle. Although the flight maneuver resulted in excursions greater than planned, the control system did manage to damp out the oscillation in less than 1 min. With a less conservative design approach, the resulting entry maneuver could have been a good deal worse.

To assess the problem with the first bank maneuver, the flight-determined stability and control derivatives were compared with the predictions. Of all the derivatives obtained from STS-1, the two important ones that differed most from the predictions at the flight condition being discussed were C_{ℓ_β} and the rolling moment due to yaw jet firing, L_{Y_J}. Since the entry tends to monotonically decrease in Mach number, the derivatives can be best portrayed as functions of the guidance system "Mach number," which is V/1000. Figure 32 shows C_{ℓ_β} as a function of guidance Mach number, and Fig. 33 shows L_{Y_J} as a function of guidance Mach number. Only the estimates from STS-1 are shown in these figures.

When only the change in C_{ℓ_β} was entered into the simulation data base, the maneuver looked very much like the original prediction (Fig. 29); however, as expected, the frequency of the oscillations changed to be more representative of the actual flight frequencies (Fig. 30). The effect on the simulation of changing only L_{Y_J} from the predictions is shown, with the flight response, in Fig. 34. These two time histories are very close, considering that the other differences between the flight-determined and predicted derivatives have been ignored.

It is apparent that the primary problem with the initial bank maneuver was the poor prediction of L_{Y_J}. The control system software is very complex, and it cannot be changed and verified between shuttle missions; therefore, an interim approach was taken to keep this large excursion from occurring on future flights. The flight-determined derivatives were put into the simulation data base, and the shuttle pilots practiced performing the maneuver manually, trying to attain a smaller response within more desirable limits. The maneuver was performed manually on STS-2 to STS-4. Figure 35 shows the manually flown maneu-

ver from STS-2. For this maneuver, roll rate, yaw rate, and sideslip angle were within the desired limits. The maneuver does not look like the original predicted response, because the derivatives and the input were different and the basic control system remained unchanged. Since the response variables were kept low and the inputs were slower and smaller, the flight responses on STS-2 to STS-4 did not show a tendency to oscillate. The software was updated for STS-5, and the resulting automated maneuver is essentially indistinguishable from that shown in Fig. 35. This maneuver has been used on all subsequent shuttle flights.

The application of parameter estimation techniques to the highly complex space shuttle vehicle will continue, and the results of this application have and will significantly affect the control system design, placard modification, and flight procedures in general.

Concluding Remarks

In this paper, the aircraft parameter estimation problem is used as an example of how parameter estimation can be applied in many scientific and engineering fields to assess phenomenology from observations, and a brief survey of the literature is presented. The theory, a simple simulated example, and the application of experimental results to solve real problems are given and explained. The maximum likelihood parameter estimation technique was used in the F-14 program to effect control system changes that improved handling qualities at high angles of attack. The same technique provided the primary source of information for control system refinement on the unstable HiMAT vehicle. Space shuttle energy-management maneuvers have been redefined based on simulations using flight-determined stability and control estimates. Moreover, parameter estimation techniques are being relied upon for future control system design, placard modification or removal, and flight procedures in general for the space shuttle.

The explanation of parameter estimation techniques and the demonstration of their highly successful application to the aircraft problems are intended to inform and to encourage scientists in other fields to consider these techniques for application to problems where a representative model and high-quality data exist.

References

[1]Iliff, Kenneth W., and Maine, Richard E., "NASA Dryden's Experience in Parameter Estimation and Its Use in Flight Test," AIAA-82-1373, AIAA AFM Conference, San Diego, California, Aug. 1982.

[2]Iliff, Kenneth W., and Maine, Richard E., "More Than You May Want to Know About Maximum Likelihood Estimation," NASA TM-85905, 1985.

[3]Zadeh, Lotfi A., and Desoer, Charles A., Linear System Theory, McGraw-Hill Book Co., New York, 1963.

[4]Schweppe, Fred C., Uncertain Dynamic Systems, Prentice-Hall, Englewood Cliffs, New Jersey, 1973.

[5]Maine, Richard E., and Iliff, Kenneth W., "Identification of Dynamic Systems," AGARD-AG-300, 1984. (Also published as NASA RP-1138, 1985.)

[6]Maine, Richard E., and Iliff, Kenneth W., "Application of Parameter Estimation to Aircraft Stability and Control — The Output-Error Approach," NASA RP-1168, 1986.

[7]Norton, F.H., "The Measurement of the Damping in Roll on a JN4h in Flight," NACA Rep. 167, 1923.

[8]Norton, F.H., "A Study of Longitudinal Dynamic Stability in Flight," NACA Rep. 170, 1923.

[9]Iliff, Kenneth W., and Maine, Richard E., "A Bibliography for Aircaft Parameter Estimation," NASA TM-86804, 1986.

[10]Gauss, Karl Friedrich, Theory of the Motion of the Heavenly Bodies Moving About the Sun in Conic Sections (translated by Charles Henry Davis, 1857), Dover Publications, Inc., New York, 1847. (Translated from Theoria Motus, 1809.)

[11]Douglas, J., "Theorems in the Inverse Problem in the Calculus of Variations," Proc. Natl. Acad. Sci., vol. 16, no. 3., 1940.

[12]Gelfand, I.M., and Levitan, B.M., "On the Determination of a Differential Equation From Its Spectral Function," Izvestiya Ac., vol. 15, no. 4, Nauk, USSR, 1951.

[13]Feldbaum, A.A., "Dual Control Theory," Automn. Remote Control, vol. 22, 1961, pp. 1-12 and 109-121.

[14]Cuenod, M., and Sage, A., "Comparison of Some Methods Used for Process Identification," Automatica, vol. 4, 1968, pp. 235-269.

[15]Balakrishnan, A.V., and Peterka, V., "Identification in Automatic Control Systems," Automatica, vol. 5, 1969, pp. 817-829.

[16]Åström, K.J., and Eykhoff, P., "System Identification — A Survey," Automatica, vol. 7, no. 2, 1971, pp. 123-162.

[17]Eykhoff, Pieter, System Identification, Parameter and State Estimation, John Wiley & Sons, London, 1974.

[18]Åström, Karl J., "Control Problems in Papermaking," Proc. IBM Scientific Computing Symposium on Control Theory and Applications, IBM Data Processing Division, White Plains, New York, 1966, pp. 135-167.

[19]Kashyap, R.L., "A New Method of Recursive Estimation in Discrete Linear Systems," IEEE Trans. Automatic Control, vol. AC-15, no. 1, Feb. 1970, pp. 18-24.

[20]Balakrishnan, A.V., "Stochastic System Identification Techniques," Stochastic Optimization and Control, H.F. Karreman, ed., John Wiley & Sons, London, 1968.

[21]Balakrishnan, A.V., "Stochastic Differential System I," Filtering and Control; A Function Space Approach, M. Beckman, G. Goos, and H.P. Kunzi, eds., Springer-Verlag, Berlin, 1973. (Lecture Notes in Economics and Mathematical Systems, vol. 84.)

[22]Balakrishnan, A.V., "Modelling and Identification Theory: A Flight Control Application," Theory and Applications of Variable Structure Systems, R.B. Mohler and A. Ruberti, eds., Academic Press, New York, 1972.

[23]Iliff, Kenneth W., "Identification and Stochastic Control With Application to Flight Control in Turbulence," Ph.D. Dissertation, Univ. of California, Los Angeles, May 1973.

[24]Maine, Richard E., and Iliff, Kenneth W., "The Theory and Practice of Estimating the Accuracy of Dynamic Flight-Determined Coefficients," NASA RP-1077, 1981.

[25]"Parameter Estimation Techniques and Applications in Aircraft Flight Testing," NASA TN D-7647, 1974.

[26]"Methods for Aircraft State and Parameter Identification," AGARD-CP-172, May 1975.

[27]Breuhaus, W.O., "Summary of Dynamic Stability and Control Flight Research Conducted Utilizing a B-25J Airplane," Rep. no. TB-405-F-10, Cornell Aeronautical Laboratory, Buffalo, New York, May 1948.

[28]Seamans, R.C., Jr., Blasingame, B.P., and Clementson, G.C., "The Pulse Method for the Determination of Aircraft Dynamic Performance," J. Aeronaut. Sci., vol. 17, no. 1, Jan. 1950, pp. 22-38.

[29]Greenberg, Harry, "A Survey of Methods for Determining Stability Parameters of an Airplane From Dynamic Flight Measurements," NACA TN-2340, 1951.

[30]Shinbrot, Marvin, "On the Analysis of Linear and Nonlinear Dynamical Systems From Transient-Response Data," NACA TN-3288, 1954.

[31]Howard, J., "The Determination of Lateral Stability and Control Derivatives From Flight Data," Can. Aeronautics Space J., vol. 13, no. 3, Mar. 1967, pp. 126-134.

[32]Wolowicz, Chester H., "Considerations in the Determination of Stability and Control Derivatives and Dynamic Characteristics From Flight Data," AGARD-AR-549, Part 1, 1966.

[33]Rampy, John M., and Berry, Donald T., "Determination of Stability Derivatives From Flight Test Data by Means of High Speed Repetitive Operation Analog Matching," FTC-TDR-64-8, Edwards, California, May 1964.

[34]Rynaski, Edmund G., "Application of Advanced Identification Techniques to Nonlinear Equations of Motion," Proc. Stall/Post-Stall/Spin Symposium, Wright-Patterson Air Force Base, Ohio, Dec. 15-17, 1971, pp. O-1 to O-18.

[35]Iliff, Kenneth W., and Taylor, Lawrence W., Jr., "Determination of Stability Derivatives from Flight Data Using a Newton-Raphson Minimization Technique," NASA TN D-6579, 1972.

[36]Taylor, Lawrence W., Jr., and Iliff, Kenneth W., "A Modified Newton-Raphson Method for Determining Stability Derivatives From Flight Data," Second International Conference on Computing Methods in Optimization Problems, San Remo, Italy, Sept. 9-13, 1968, Academic Press, New York, 1969, pp. 353-364.

[37]Larson, Duane B., and Fleck, John T., "Identification of Parameters by the Method of Quasilinearization," Report 164, Cornell Aeronautical Laboratory, Buffalo, New York, May 1968.

[38]Balakrishnan, A.V., Communication Theory, McGraw-Hill, New York, 1968.

[39]Bellman, Richard E., and Kalaba, Robert E., Quasilinearization and Nonlinear Boundary-Value Problems, American Elsevier Publishing Co., New York, 1965.

[40]Taylor, Lawrence W., Jr., Iliff, Kenneth W., and Powers, Bruce, G., "A Comparison of Newton-Raphson and Other Methods for Determining Stability Derivatives From Flight Data," AIAA-69-315, Mar. 1969.

[41]Grove, Randall D., Bowles, Roland L., and Mayhew, Stanley C., "A Procedure for Estimating Stability and Control Parameters From Flight Test Data by Using Maximum Likelihood Methods Employing a Real-Time Digital System," NASA TN D-6735, 1972.

[42]Ross, A. Jean, and Foster, G.W., "FORTRAN Programs for the Determination of Aerodynamic Derivatives From Transient Longitudinal or Lateral Responses of Aircraft," TR-75090, Royal Aircraft Establishment, Sept. 1975.

[43]Maine, Richard E., and Iliff, Kenneth W., "A FORTRAN Program for Determining Aircraft Stability and Control Derivatives From Flight Data," NASA TN D-7831, 1975.

[44]Nagy, Christopher J., "A New Method for Test and Analysis of Dynamic Stability and Control," AFFTC-TD-75-4, Air Force Flight Test Center, Edwards, California, May 1976.

[45]Iliff, Kenneth W., Maine, Richard E., and Shafer, Mary F., "Subsonic Stability and Control Derivatives for an Unpowered, Remotely Piloted 3/8-scale F-15 Airplane Model Obtained From Flight Test," NASA TN D-8136, 1976.

[46]Sim, Alex G., "A Correlation Between Flight-Determined Derivatives and Wind-Tunnel Data for the X-24B Research Aircraft," NASA SX-3371, 1976.

[47]Jeglum, Paul M., "AFFTC Experience in the Use of Flight-Test Derived Stability Derivatives," Paper 14, AGARD Fluid Dynamics Panel Symposium on Dynamic Stability Parameters, Athens, Greece, May 22-24, 1978.

[48]Holleman, Euclid C., "Summary of Flight Tests to Determine the Spin and Controllability Characteristics of a Remotely Piloted, Large-Scale (3/8) Fighter Airplane Model," NASA TN D-8052, 1976.

[49]Smith, Harriet J., "Flight-Determined Stability and Control Derivatives for an Executive Jet Transport," NASA TM X-56034, 1975.

[50]Suit, William T., "Aerodynamic Parameters of the Navion Airplane Extracted From Flight Data," NASA TN D-6643, 1972.

[51]Frei, D.R., "Practical Applications of Parameter Identification," AIAA-77-1136, Aug. 1977.

[52]Ross, A. Jean, "Determination of Aerodynamic Derivatives From Transient Response in Manoeuvring Flight," Methods for Aircraft State and Parameter Identification, AGARD-CP-172, May 1975, pp. 14-1 to 14-10.

[53]Gould, D.G., and Hindson, W.S., "Estimates of the Stability Derivatives of a Helicopter and a V/STOL Aircraft From Flight Data," Methods for Aircraft State and Parameter Identification, AGARD-CP-172, May 1975, pp. 23-1 to 23-9.

[54]Klein, V., "Longitudinal Aerodynamic Derivatives of a Slender Delta-Wing Research Aircraft Extracted From Flight Data," CIT-FI-74-023, Cranfield Inst. of Technology, July 1974.

[55]Schuetz, A.J., "Low Angle-of-Attack Longitudinal Aerodynamic Parameters of Navy T-2 Trainer Aircraft Extracted From Flight Data: A Comparison of Identification Technique. Volume I – Data Acquisition and Modified Newton-Raphson Analysis," NADC-74181-30-VOL-1 AD-A013181, Naval Air Development Center, Warminster, Pennsylvania, June 1975.

[56]Marchand, M., and Koehler, R., "Determination of Aircraft Derivatives by Automatic Parameter Adjustment and Frequency Response Methods," Methods for Aircraft State and Parameter Identification, AGARD-CP-172, May 1975, pp. 17-1 to 17-18.

[57]"Dynamic Stability Parameters," AGARD-CP-235, 1978.

[58]"Parameter Identification," AGARD-LS-104, 1979.

[59]Mehra, Raman K., "Maximum Likelihood Identification of Aircraft Parameters," Eleventh Joint Automatic Control Conference of the American Automatic Control Council, Paper 18-C, June 1970, pp. 442-444.

[60]Tyler, James S., Powell, J. David, and Mehra, Raman K., "The Use of Smoothing and Other Advanced Techniques for VTOL Aircraft Parameter Identification. Final Report," Naval Air Systems Command Contract No. N00019-69-C-0534, Systems Control, Inc., Palo Alto, California, June 1970.

[61]Gerlach, O.H., "The Determination of Stability Derivatives and Performance Characteristics From Dynamic Manoeuvres," Rep. VTH-163, Delft Univ. of Technology, Dept. of Aerospace Engineering, Delft, The Netherlands, Mar. 1971.

[62]Jonkers, H.L., "Application of the Kalman Filter to Flight Path Reconstruction From Flight Test Data Including Estimation of Instrumental Bias Error Corrections," Report VTH-162, Delft Univ. of Technology, Dept. of Aerospace Engineering, Delft, The Netherlands, Feb. 1976.

[63]Chen, Robert T.N., and Eulrich, Bernard J., "Parameter and Model Identification of Nonlinear Dynamical Systems Using a Suboptimal Fixed-Point Smoothing Algorithm," Twelfth Joint Automatic Control Conference of the American Automatic Control Council, Paper 7-E2, Aug. 1971, pp. 731-740.

[64]Yazawa, Kenji, "Identification of Aircraft Stability and Control Derivatives in the Presence of Turbulence," AIAA-77-1134, Aug. 1977.

[65]Iliff, Kenneth W., and Maine, Richard E., "Practical Aspects of Using a Maximum Likelihood Estimator," Methods for Aircraft State and Parameter Identification, AGARD-CP-172, Paper 16, May 1975, pp. 16-1 to 16-15.

[66]Iliff, Kenneth W., and Maine, Richard E., "Further Observations on Maximum Likelihood Estimates of Stability and Control Characteristics Obtained From Flight Data," AIAA-77-1133, Aug. 1977.

[67]Maine, Richard E., and Iliff, Kenneth W., "User's Manual for MMLE3, A General FORTRAN Program for Maximum Likelihood Parameter Estimation," NASA TP-1563, 1980.

[68]Maine, Richard E., and Iliff, Kenneth W., "Formulation and Implementation of a Practical Algorithm for Parameter Estimation With Process and Measurement Noise," SIAM J. Appl. Math., vol. 41, no. 3, Dec. 1981, pp. 558-579.

[69]Maine, Richard E., and Murray, James E., "Application of Parameter Estimation to Highly Unstable Aircraft," AIAA-86-2020-CP, 1986. (Also published as NASA TM-88266, 1986.)

[70]Nguyen, Luat T., Gilbert, William P., Gera, Joseph, Iliff, Kenneth W., and Enevoldson, Einar K., "Application of High-Alpha Control System Concepts to a Variable-Sweep Fighter Airplane," AIAA-80-1582, Aug. 1980.

[71]Gera, Joseph, Wilson, R.J., and Enevoldson, E.K., "Flight Test Experience With High-α Control System Techniques on the F-14 Airplane," AIAA-81-2505, Nov. 1981.

[72]Gera, Joseph, "Simulation as an Analysis Tool in Flight Testing a Modified Control System on the F-14 Airplane," SES/SFTE Simulation-Aircraft Test and Evaluation Symposium, Patuxent River, Mar. 16-17, 1982.

[73]Gingrich, P.B., Child, R.D., and Panageas, G.N., "Aerodynamic Configuration Development of the Highly Maneuverable Aircraft Technology Remotely Piloted Research Vehicle," NASA CR-143841, 1977.

[74]Petersen, Kevin L., "Flight Control Systems Development of Highly Maneuverable Aircraft Technology (HiMAT) Vehicle," AIAA-79-1789, Aug. 1979.

[75]Matheny, Neil W., and Panageas, George N., "HiMAT Aerodynamic Design and Flight Test Experience," AIAA-81-2433, Nov. 1981.

[76]Cooke, Douglas R., "Space Shuttle Stability and Control Flight Test Techniques," AIAA-80-1608, Aug. 1980.

[77]Young, James C., and Underwood, Jimmy M., "The Development of Aerodynamic Uncertainties for the Space Shuttle Orbiter," AIAA-82-0563, Mar. 1982.

[78]Weil, Joseph, and Powers, Bruce G., "Correlation of Predicted and Flight Derived Stability and Control Derivatives — With Particular Application to Tailless Delta Wing Configurations," NASA TM-81361, 1981.

[79]Iliff, Kenneth W., Maine, Richard E., and Cooke, Douglas R., "Selected Stability and Control Derivatives From the First Space Shuttle Entry," AIAA-81-2451, Nov. 1981.

[80]Maine, Richard E., and Iliff, Kenneth W., "Selected Stability and Control Derivatives from the First Three Space Shuttle Entries," AIAA-81-1318, Aug. 1982.

Table 1 Pertinent values as a function of iteration

L	$\hat{L}_p(L)$	$\hat{L}_\delta(L)$	$\phi(L)$	$\psi(L)$	J_L
0	-0.5000	15.00	0.9048	2.855	21.21
1	-0.3005	9.888	0.9417	1.919	0.5191
2	-0.2475	9.996	0.9517	1.951	5.083×10^{-4}
3	-0.2500	10.00	0.9512	1.951	1.540×10^{-9}
4	-0.2500	10.00	0.9512	1.951	1.060×10^{-14}

Table 2 Pertinent values as a function of iteration

L	$\hat{L}_p(L)$	$\hat{L}_\delta(L)$	$\phi(L)$	$\psi(L)$	J_L
0	-0.5000	15.00	0.9048	2.855	30.22
1	-0.3842	10.16	0.9260	1.956	3.497
2	-0.3518	10.23	0.9321	1.976	3.316
3	-0.3543	10.25	0.9316	1.978	3.316
4	-0.3542	10.24	0.9316	1.978	3.316
5	-0.3542	10.24	0.9316	1.978	3.316

Table 3 Mean and standard deviations for estimates of L_p

Number of cases, N	Sample mean, $\mu(\hat{L}_p)$	Sample standard deviation, $\sigma(\hat{L}_p)$	Standard deviation of the sample mean, $\sigma(\hat{L}_p)/\sqrt{N}$
5	-0.2668	0.0739	0.0336
10	-0.2511	0.0620	0.0196
20	-0.2452	0.0578	0.0129

Table 4 Estimates of L_p and Cramér-Rao bound as functions of the square root of noise power

Square root of noise power, G	Estimate of L_p	Cramér-Rao bound
0.0	-0.2500	---
0.01	-0.2507	0.00054
0.05	-0.2535	0.00271
0.10	-0.2570	0.00543
0.2	-0.2641	0.0109
0.4	-0.2783	0.0220
0.8	-0.3071	0.0457
1.0	-0.3218	0.0579
2.0	-0.3975	0.1248
5.0	-0.6519	0.3980
10.0	-1.195	1.279

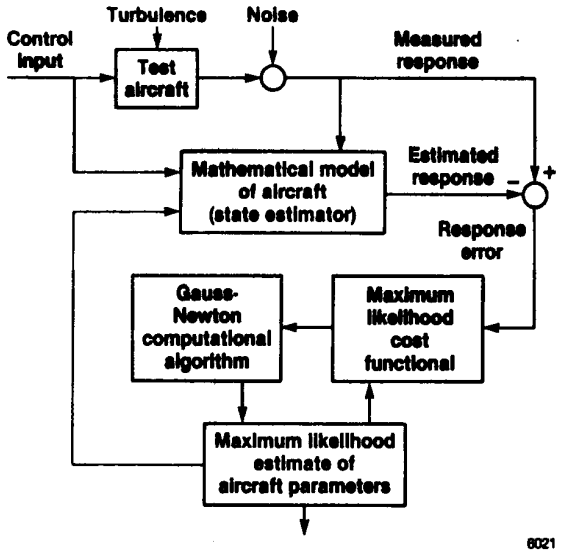

Fig. 1 Maximum likelihood estimation concept.

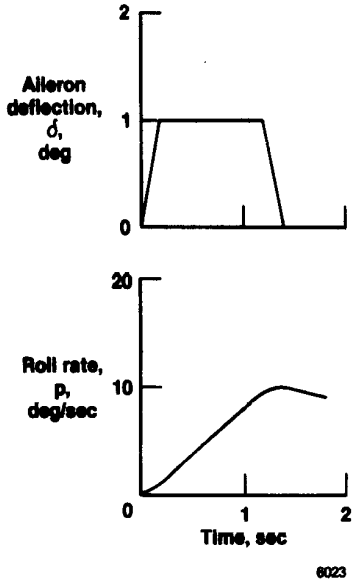

Fig. 3 Time history with no measurement noise.

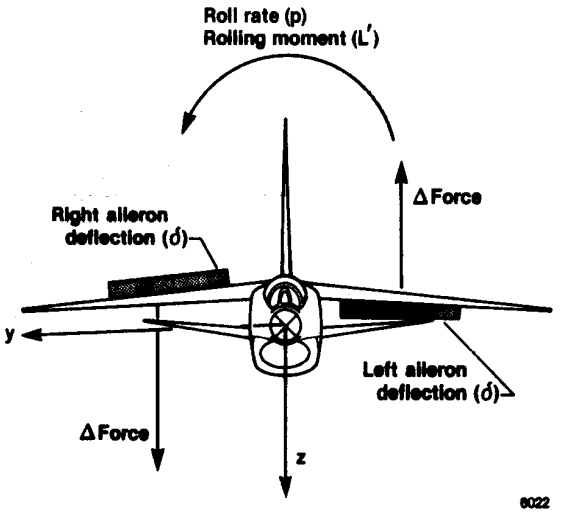

Fig. 2 Simplified aircraft nomenclature.

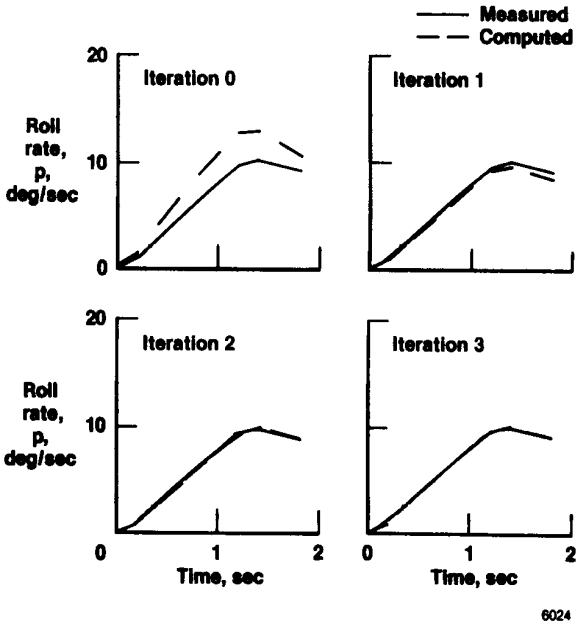

Fig. 4 Comparison of simulated measured and estimated data for each of the first three iterations for no-noise case.

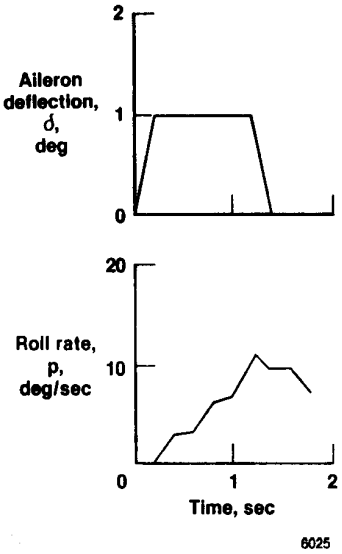

Fig. 5 Time history with measurement noise.

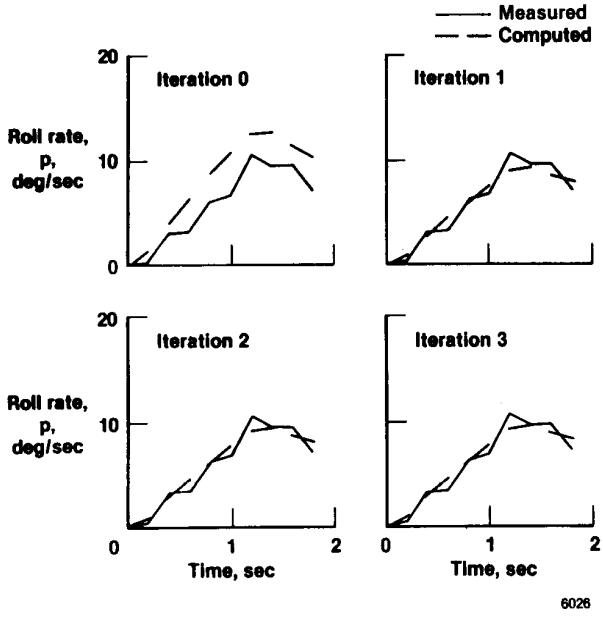

Fig. 6 Comparison of simulated measured and estimated data for each iteration for noisy case.

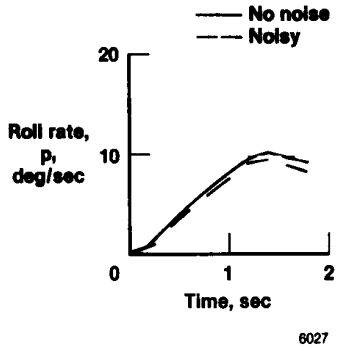

Fig. 7 Comparison of estimated roll rate from no-noise and noisy cases.

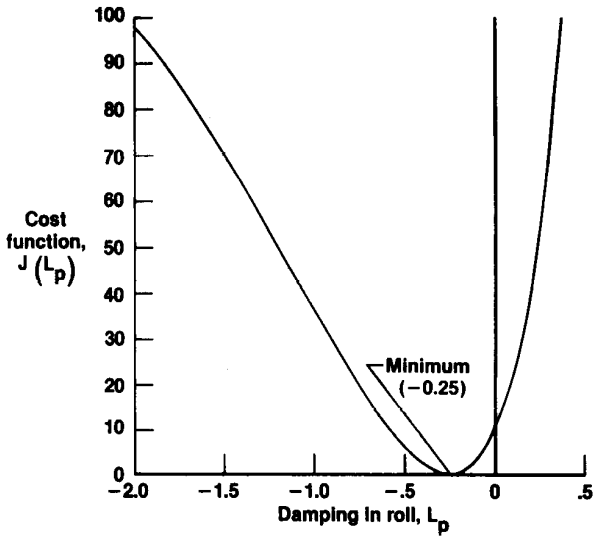

Fig. 8 Cost function $J(L_p)$ as a function of L_p for no-noise case.

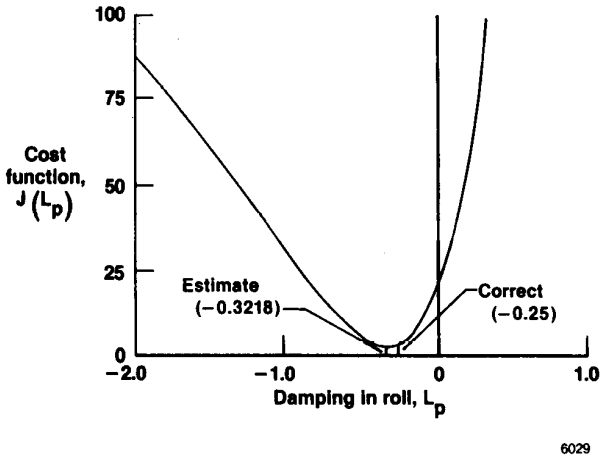

Fig. 9 Cost function $J(L_p)$ as a function of L_p for noisy case.

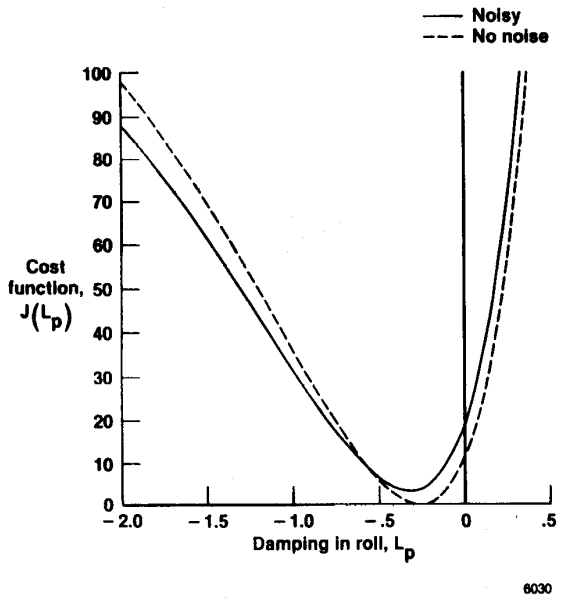

Fig. 10 Comparison of the cost functions for no-noise and noisy cases.

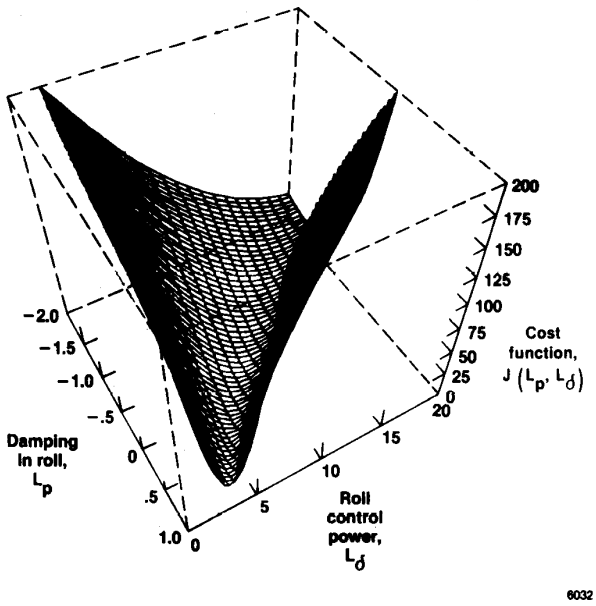

Fig. 12 Restricted view of cost function surface.

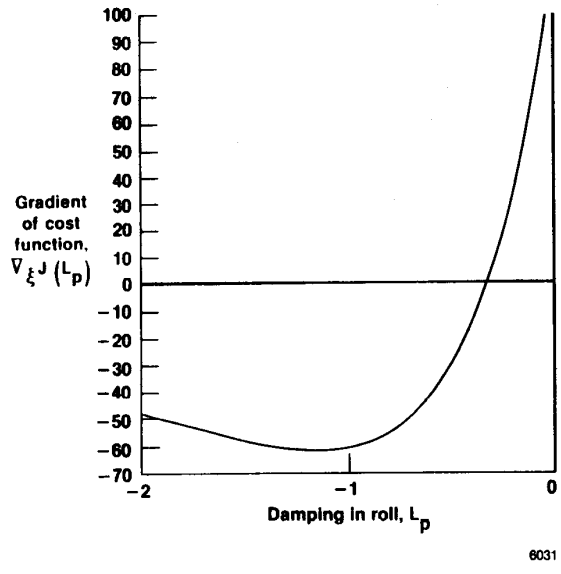

Fig. 11 Gradient of $J(L_p)$ as a function of L_p for noisy case.

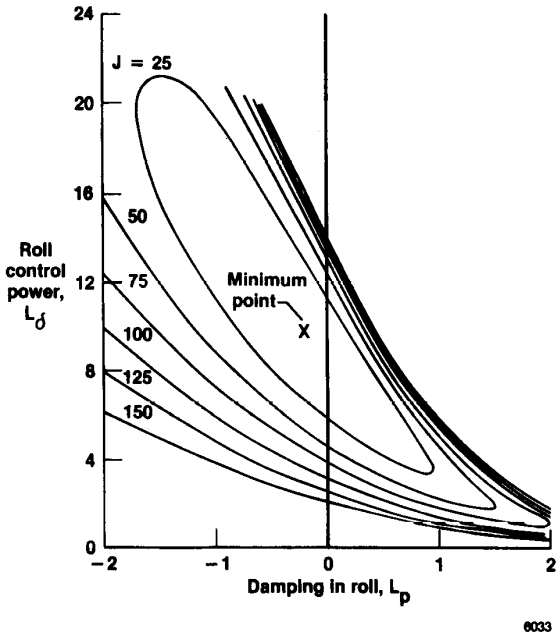

Fig. 13 Isoclines of constant cost in L_p and L_δ for no-noise case.

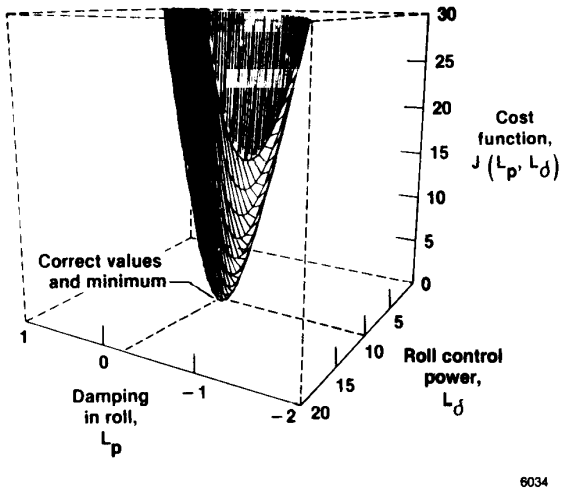

Fig. 14 Detailed view of cost function surface for no-noise case.

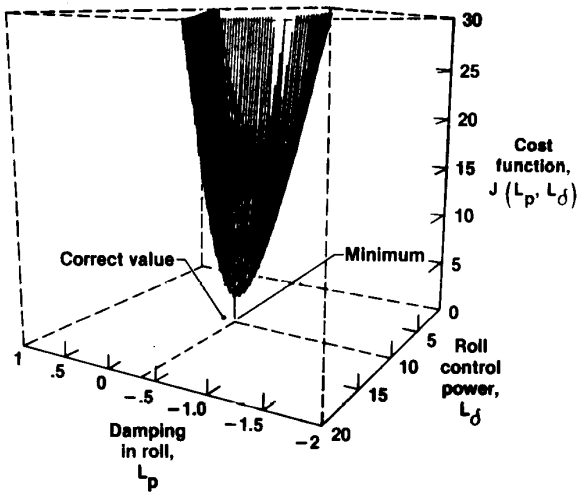

Fig. 16 Detailed view of cost function surface for noisy case.

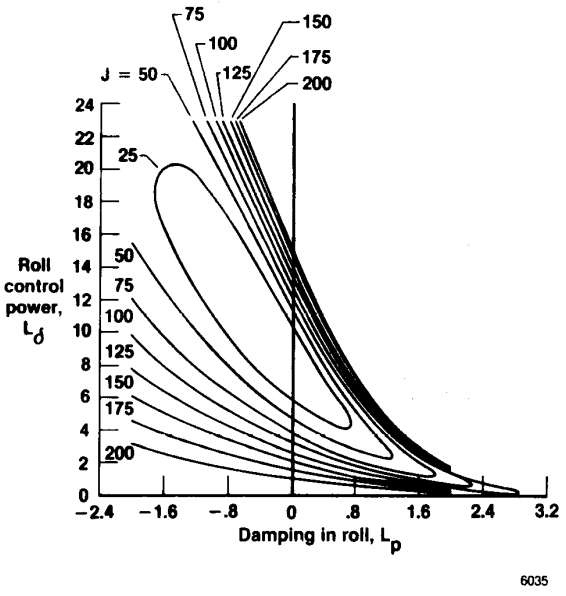

Fig. 15 Isoclines of constant cost in L_p and L_δ for noisy case.

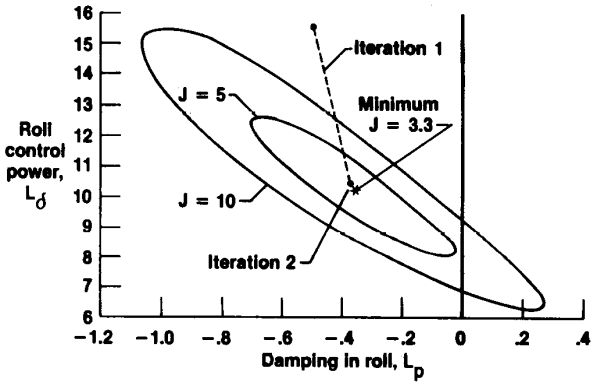

Fig. 17 Isoclines of constant cost in region near minimum for noisy case.

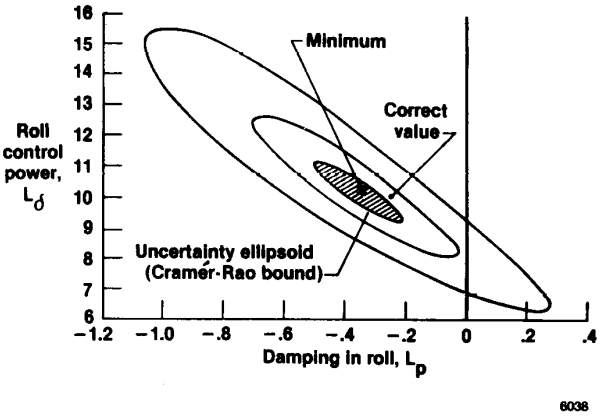

Fig. 18 Isoclines and uncertainty ellipsoid of the cost function for noisy case.

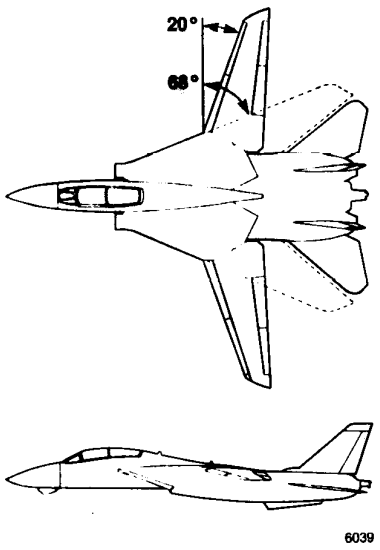

Fig. 19 F-14 airplane configuration.

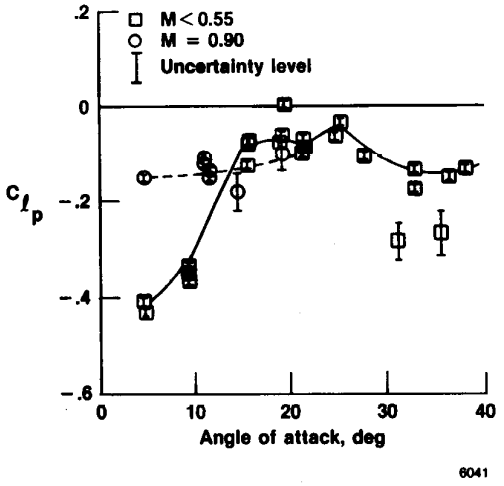

Fig. 21 Summary of flight-derived estimates of roll damping for M < 0.55 and M = 0.9.

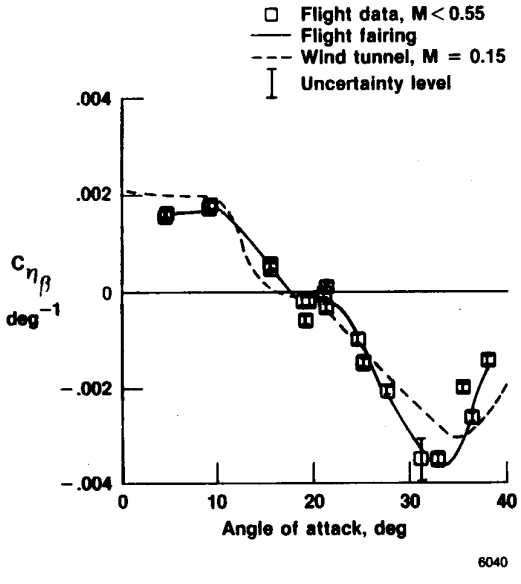

Fig. 20 Comparison of flight-derived estimates of static directional stability with wind tunnel data.

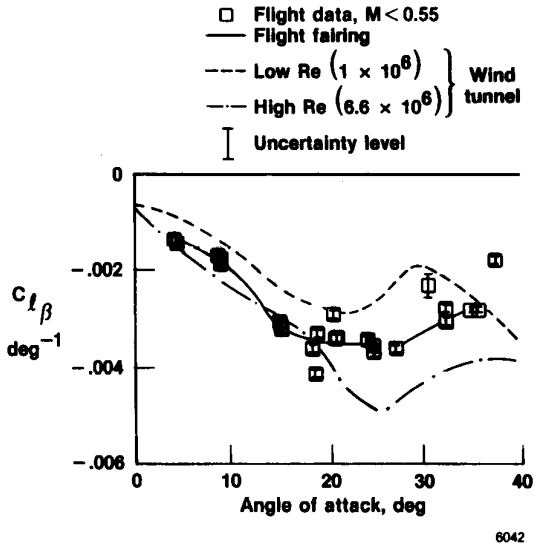

Fig. 22 Comparison of flight-derived estimates of dihedral effect with two sets of wind tunnel data.

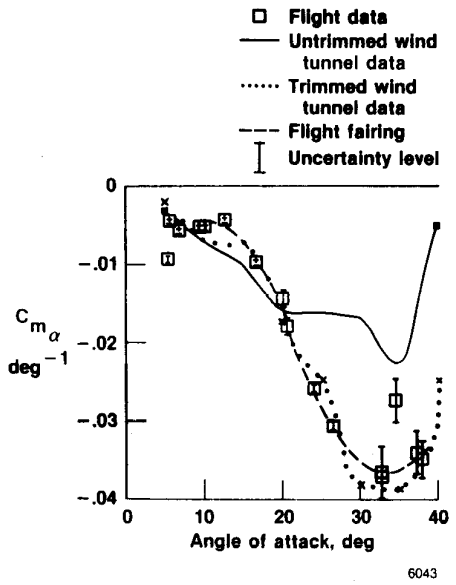

Fig. 23 Comparison of flight and wind tunnel estimates for C_{m_α}.

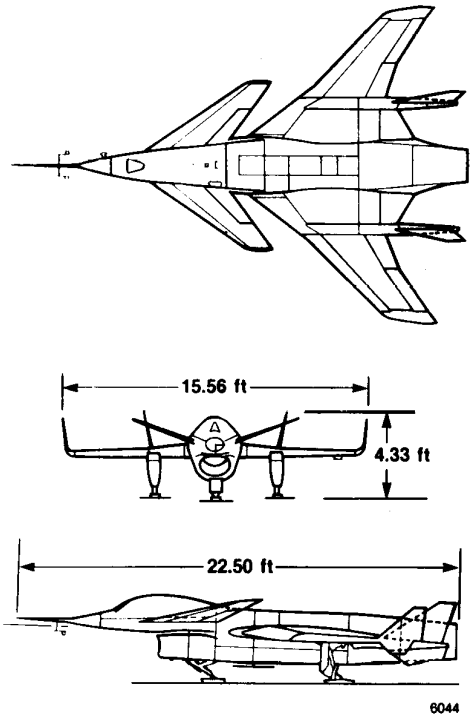

Fig. 24 HiMAT remotely piloted research vehicle baseline configuration.

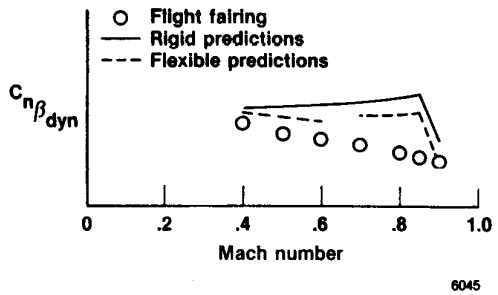

Fig. 25 Comparison of flight and predicted estimates for directional dynamic stability at α = 4° as a function of Mach number.

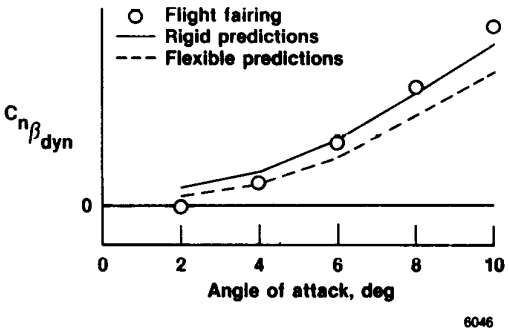

Fig. 26 Comparison of flight and predicted estimates for directional dynamic stabilty as a function of angle of attack at M = 0.9.

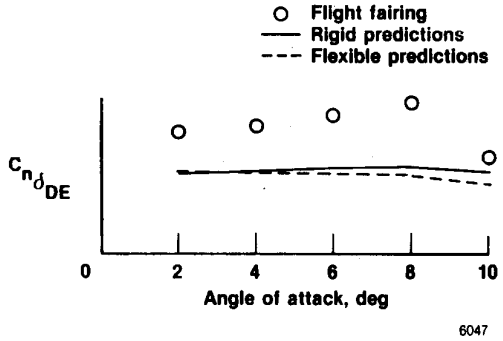

(a) Differential elevon yawing moment coefficient.

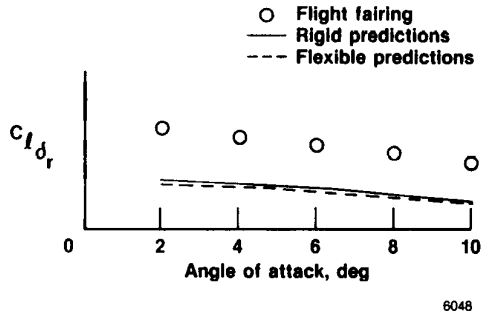

(b) Rudder rolling moment coefficient.

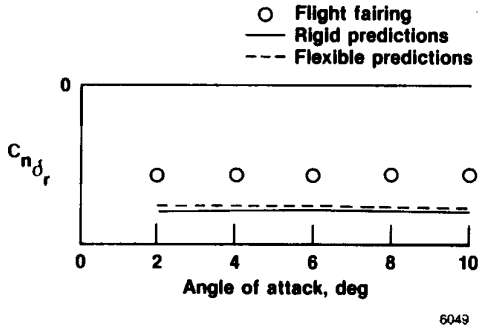

(c) Rudder yawing moment coefficient.

Fig. 27 Comparison of selected control derivatives as functions of angle of attack at M = 0.9.

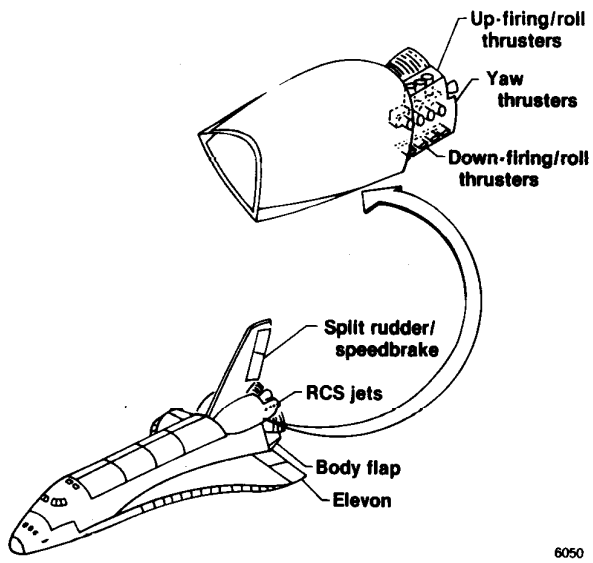

Fig. 28 Shuttle configuration.

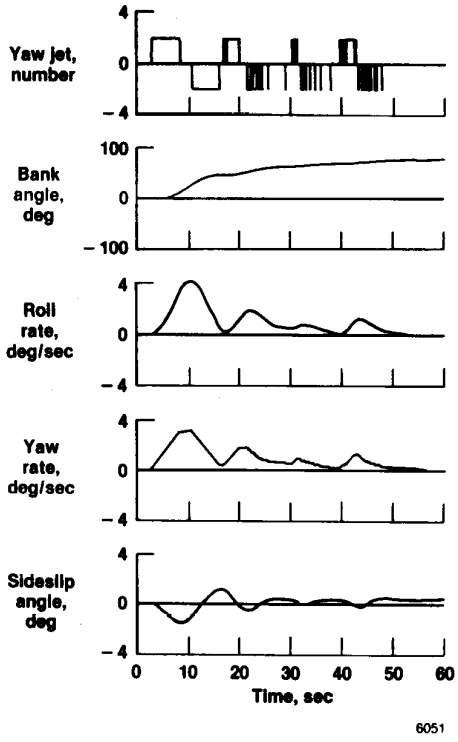

Fig. 29 Predicted STS-1 bank maneuver at M = 24.

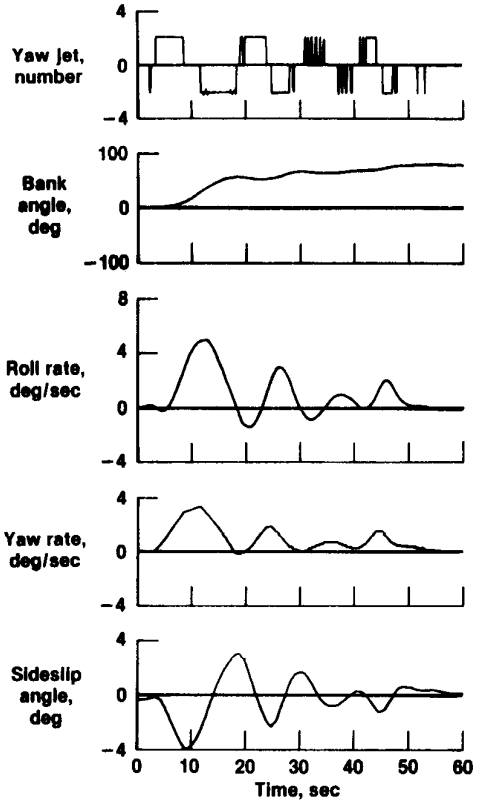

Fig. 30 Actual STS-1 bank maneuver at M = 24.

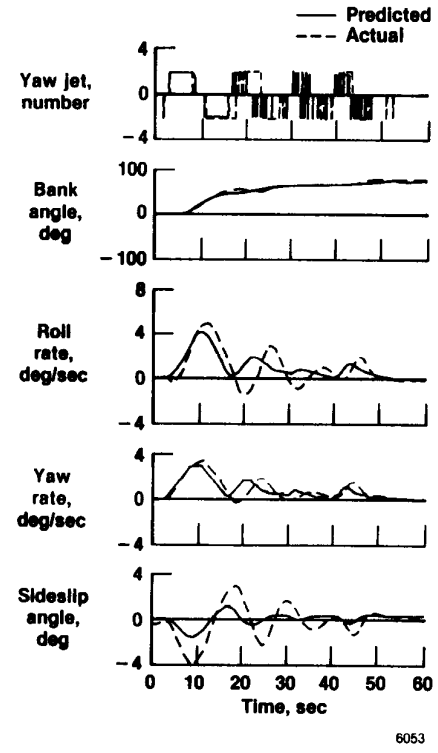

Fig. 31 Comparison of actual and predicted STS-1 bank maneuver.

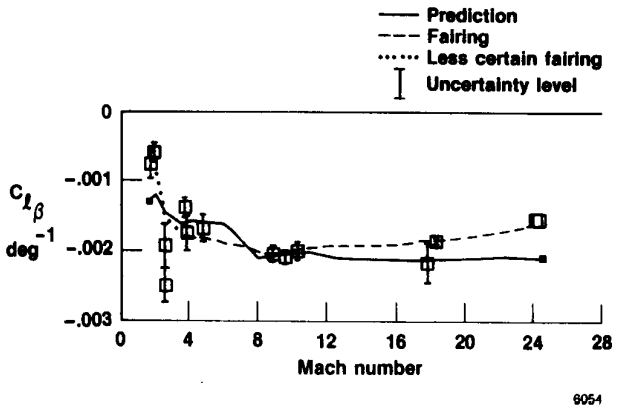

Fig. 32 Estimates of dihedral effect for the space shuttle.

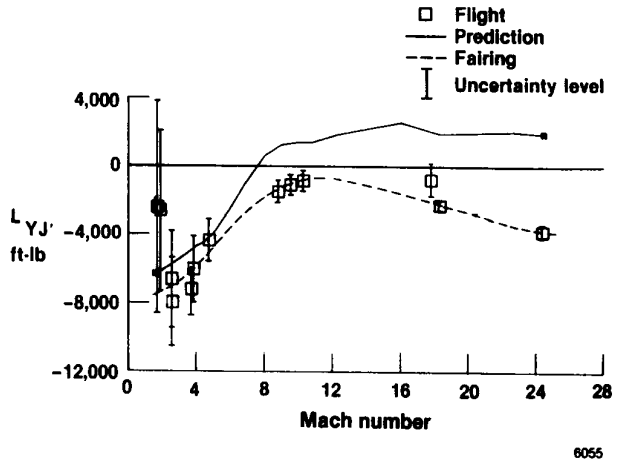

Fig. 33 Estimates of L_{YJ} for the space shuttle.

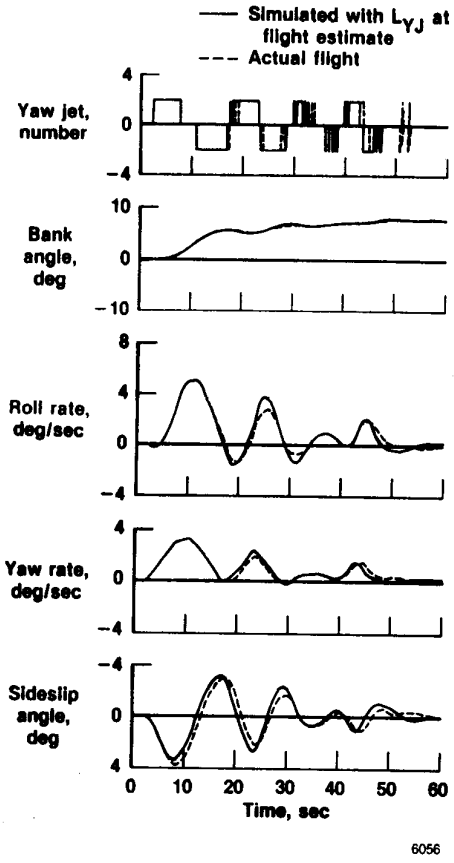

Fig. 34 Comparison of simulated bank maneuver with L_{YJ} at a flight-estimated value with the actual STS-1 bank maneuver.

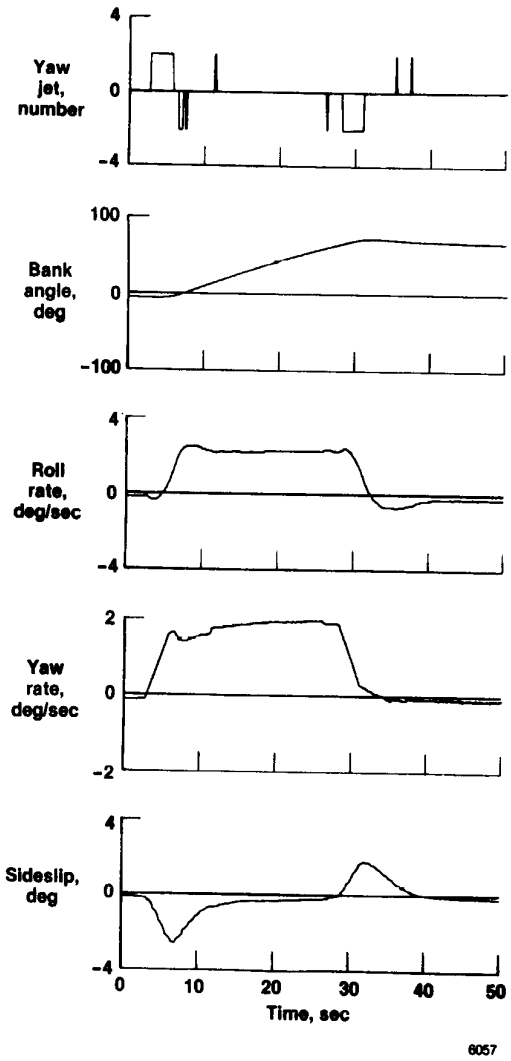

Fig. 35 Manual bank maneuver at M = 24 from STS-2.

1. Report No.	2. Government Accession No.	3. Recipient's Catalog No.
NASA TM-88281		

4. Title and Subtitle	5. Report Date
AIRCRAFT PARAMETER ESTIMATION — AIAA DRYDEN LECTURE IN RESEARCH FOR 1987	January 1987
	6. Performing Organization Code
7. Author(s)	8. Performing Organization Report No.
Kenneth W. Iliff	H-1394
	10. Work Unit No.
9. Performing Organization Name and Address	RTOP 505-61
NASA Ames Research Center Dryden Flight Research Facility P.O. Box 273 Edwards, CA 93523-5000	11. Contract or Grant No.
	13. Type of Report and Period Covered
12. Sponsoring Agency Name and Address	Technical Memorandum
National Aeronautics and Space Administration Washington, D.C. 20546	14. Sponsoring Agency Code

15. Supplementary Notes

Prepared as the AIAA Dryden Lecture in Research paper, to be presented at the AIAA 25th Aerospace Sciences Meeting, Reno, Nevada, January 12-15, 1987.

16. Abstract

The aircraft parameter estimation problem is used to illustrate the utility of parameter estimation, which applies to many engineering and scientific fields. Maximum likelihood estimation has been used to extract stability and control derivatives from flight data for many years. This paper presents some of the basic concepts of aircraft parameter estimation and briefly surveys the literature in the field. The maximum likelihood estimator is discussed, and the basic concepts of minimization and estimation are examined for a simple simulated aircraft example. The cost functions that are to be minimized during estimation are defined and discussed. Graphic representations of the cost functions are given to illustrate the minimization process. Finally, the basic concepts are generalized, and estimation from flight data is discussed. Some of the major conclusions for the simulated example are also developed for the analysis of flight data from the F-14, highly maneuverable aircraft technology (HiMAT), and space shuttle vehicles.

17. Key Words (Suggested by Author(s))	18. Distribution Statement
Aircraft flight testing Aircraft stability and control Maximum likelihood Parameter estimation	Unclassified — Unlimited Subject category 05

19. Security Classif. (of this report)	20. Security Classif. (of this page)	21. No. of Pages	22. Price*
Unclassified	Unclassified	27	A03

*For sale by the National Technical Information Service, Springfield, Virginia 22161.